An Operational Computational Terminal Area PBL Prediction System

NASA Grant NCC-1-220

Calender Year 96 Annual Report

submitted to the
NASA Langley Research Center

Dr. Yuh-Lang Lin
Dr. Michael L. Kaplan
Dr. Ronald P. Weglarz
Mr. David W. Hamilton

Department of Marine, Earth, and Atmospheric Sciences
North Carolina State University
Raleigh, North Carolina 27695-8208
Tel:/FAX: (919)515-1438 /1683

February 1997

Table of Contents

1. Objectives and Goals of the Research

There are two fundamental goals of this research project which are listed here in terms of priority, i. e., a primary and a secondary goal. The first and primary goal is to develop a prognostic system which could satisfy the operational weather prediction requirements of the meteorological subsystem within the Aircraft Vortex Spacing System (AVOSS). The secondary goal is to perform indepth diagnostic analyses of the meteorological conditions affecting the Memphis field experiment held during August 1995. These two goals are interdependent because a thorough understanding of the atmospheric dynamical processes which produced the unique meteorology during the Memphis deployment will help us design a prognostic system for the planetary boundary layer (PBL) which could be utilized to support the meteorological subsystem within AVOSS.

The secondary goal occupied much of the first year of the research project. This involved extensive data acquisition and indepth analyses of a spectrum of atmospheric observational data sets to be described in Section 2, below. Concerning the primary goal, the first part of the four-stage prognostic system in support of AVOSS entitled: *"Terminal Area PBL Prediction System (TAPPS)"* was also formulated and tested in a research environment during 1996. We will describe this system, and the three stages which are planned to follow, in subsequent sections of this report. This first part of a software system designed to meet the primary goal of this research project is relatively inexpensive to implement and run operationally.

2. Work Accomplished During the Period 2/96-1/97

2.1 Meteorological Analyses of the Memphis 95 Deployment Days

2.1.1 Analyses Overview

In an effort to diagnose the meteorology during August 1995 over and surrounding Memphis, Tennessee, we compiled and analysed atmospheric data from a spectrum of operational systems. This was necessary because the weather at a specific location, such as Memphis, is affected by circulations with a variety of length (L) and time scales (τ) from the synoptic scale, i. e., L >1000 km and τ~days, to the mesoscale, i. e., L<1000 km and τ~hours, to the microscale, i. e., L<10km and τ~minutes. These data included conventional observations routinely collected by the National Weather Service (NWS) such as: (1) 12 hour rawinsonde balloon temperature and dewpoint soundings and vertical wind profiles, (2) hourly surface aviation temperature, dewpoint, and wind observations, and (3) wind profiles from the operational wind profiler sites. Also integrated into our analyses were the 5 minute wind and temperature data sets from a variety of sensors at Memphis during each deployment which were compiled by the MIT Lincoln Laboratory. These 5 minute data were used to construct time sections of key wind shear and turbulence indicators. The sensors utilized for the 5 minute data sets included profilers, balloons, sodars, and data from an instrumented tower.

The results of these analyses were intercompared for each day during August 1995 to determine if there was a relationship between persistent atmospheric circulations surrounding Memphis and the vertical wind shear and vertical temperature lapse rates observed at Memphis during the deployment days. Specifically, we were very interested in what caused the vertical wind shear and temperature lapse rates observed during the aircraft "pushes". A pressure pattern was diagnosed which likely affected the PBL wind circulations over much of the midcontinental region, i. e., the region from the Front Range of the Rocky Mountains to the Appalachian Mountains. It is likely that this circulation pattern occurs most frequently during the warm season, i. e. April though September. This circulation pattern results in nocturnal PBL jet formation which likely affects much of the

midcontinental region including Memphis from just after sunset through the morning time period.

2.1.2 Basic Climatological Processes and PBL Nocturnal Jetogenesis

To understand the basic climatology of why this nocturnal PBL jet forms, a brief description of Figs. 1 and 2 are necessary. It is a well-known fact of meteorology that during the cold season the radiation budget of the North American continent is controlled by the substantial meridional, i. e., north-south variation of incident short wave (solar) insolation. This results in a dominant meridional variation in surface temperature (Fig. 1a). What is less well-known by most nonmeteorologists, in particular, is the fact that a second radiation budget perturbation exists due to the unique geography of the North American continent. Air over the elevated plateau of the southwestern U. S. tends to warm up more, particularly in summer, than air further east over the Gulf of Mexico. This is a reflection of the fact that the air over the southwest, i. e., primarily Arizona, New Mexico, and northern Mexico, is affected by an elevated arid region. Since it is dry and elevated, much more solar insolation can heat this region when compared to the region back east which is much lower and much wetter. Air of maritime origin over the Gulf of Mexico is so moist that it is accompanied by much more cloudiness, thus reducing the incoming solar radiation. Also, since land areas heat and cool much more rapidly than maritime areas do, the southwestern (continental) air mass heats and cools on a much more rapid cycle than does the Gulf of Mexico (maritime) air mass. These regions, i. e., the arid elevated southwest desert and the moist Gulf of Mexico become source regions for air masses of uniquely different characteristics. This is reflected in the mean July surface temperatures depicted in Fig. 1b indicating a dominant zonal, i. e., west to east variation, in contradistinction to the north to south or meridional temperature variation during January. As source regions, the arid southwestern plateau and Gulf of Mexico produce changes in PBL characteristics which become quite evident when these air masses are exposed to the diurnal radiational cycle. This simply means that they warm and cool at very different rates when exposed to direct

solar heating and nocturnal long wave radiational cooling. Thus, it is the frequency and geographical distribution of each air mass, i. e., the continental and Gulf maritime air mass, which controls the summertime weather in North America rather than the broad synoptic scale meridional variation in air mass type alone. Furthermore, adding complexity to this already complex issue, is the fact that these air masses occupy smaller mesoscale volumes than do the massive air masses during the cold season. Therefore, their effect upon smaller regions is harder to diagnose and predict.

Since the continental air over the southwest warms more rapidly during the day and cools more rapidly at night when compared to the Gulf of Mexico maritime air mass, the locations of these air masses can have a profound effect on the PBL temperature and pressure gradients which can often overwhelm the synoptic scale circulation during the warm season. These PBL pressure gradients can control the low-level wind fields, thus producing mesoscale vertical wind shear zones which could have a profound effect upon the production of turbulence at local terminal areas. This is because the vertical wind shears occur very close to the ground at a level similar to those observed during the Memphis 95 deployment. In effect, wherever these air masses are juxtaposed to one another, local thermally direct circulations develop within the PBL wherein the cooler denser air flows towards the warmer less denser air. At night, this means that local pressure gradients are established which transport the cooler, drier continental air towards the warmer, wetter maritime air while during the day just the opposite occurs. Hence, the shallow PBL jets reflect the different pressure gradients established by these different air masses which warm and cool at different rates close to the earth's surface. Furthermore, kinetic energy generated by the pressure gradient force in between the continental and maritime air masses is influenced by the Coriolis force which further modifies the direction of the air flow, and, hence the jet structure. As will be described in the next section, such shallow PBL jet streams played a key role in the nighttime meteorology over Memphis during August 1995.

2.1.3 Case Study Intercomparisons of PBL Jetogenesis Formation

We will now proceed to demonstrate how this aforementioned phenomenon, i. e., nocturnal PBL jetogenesis, controlled much of the nocturnal meteorology during the August 1995 deployment at Memphis. We will do this by comparing four different case studies which demonstrate strong, moderate, and weak signals of nocturnal PBL jet formation, i. e., the 15, 16 and 11 August nights, respectively, as well as a case study wherein a synoptic scale circulation dominated the mesoscale circulations, i. e., the 24 August night. Two of these case studies, i. e., 15 and 16 August, were important nights because of the strong vertical wind shears observed during the aircraft pushes. As will be seen, these vertical wind shears are controlled by the low-level PBL jets.

Before intercomparing these case studies, however, we present in Fig. 3, the location of the rawinsonde and surface observational sites employed in these analyses. Two vertical cross sections where rawinsonde observations were utilized to calculate wind and temperature profiles are designated by dashed lines on Fig. 3. The first and most referenced cross section is from Topeka, Kansas (TOP) to Tallahassee, Florida (TLH), while a second cross section is located from Dayton, Ohio (DAY) to Corpus Christi, Texas (CRP). Rawinsonde data utilized for these analyses were derived from stations which have a number under the location identifier, while surface analyses were derived from all identified stations. For example, along the vertical cross section from TOP to TLH are stations 72456 (TOP), 72440 (Springfield, Missouri (SGF)), 72340 (Little Rock, Arkansas (LIT)), 72334 (Memphis, Tennessee (MEM) when available), 72235 (Jackson, Mississippi (JAN)), and 72214 (TLH). At each rawinsonde site the vertically interpolated wind observation is plotted at 50 mb locations. This vertically interpolated field was then horizontally interpolated along the cross section. Where terrain existed, these data where linearly interpolated down to 0 m in elevation mean sea level. We will now proceed to intercompare these case studies in an effort to diagnose the key nocturnal jetogenesis

"signals" employing conventional NWS rawinsonde and surface observations, followed by the Memphis deployment data sets.

First, the rawinsonde data intercomparisons. Figures 4-7 depict potential temperature (solid in K) and wind velocity (dotted in ms^{-1}) along the vertical cross sections from TOP to TLH. These cross sections are shown at two different times, i. e., 0000 UTC and 1200 UTC, thus reflecting the early evening and early morning temperature and wind fields, respectively, below 850 mb (<1500 m in elevation). A close inspection of Figs. 4-6 intercomparing the 15, 16, and 11 August case studies reveals an unambigous signal of nocturnal jetogenesis within the PBL. This signal is centered above LIT in the layer between 980 and 950 mb (from about 200-500 m above mean sea level) since the fields have been interpolated to sea level in the regions of higher surface elevations at TOP and SGF. An intercomparison among the three case studies shows a reduction in the intensity of the nocturnal jet maximum from ~19 ms^{-1}, to ~8 ms^{-1}, to ~4 ms^{-1} for the 15, 16, and 11 August case studies, respectively. Consistent with the development of these PBL jets, which are generally blowing from the west-southwest, are the developing cool, shallow layers from LIT northwestward to TOP wherein overnight radiational cooling within the drier continental air mass to the northwest has resulted in differential cooling to the west of MEM, thus increasing the mean sea level surface pressures to the west of where these low-level PBL jets form, i. e., generally between LIT and MEM.

This near surface cooling is consistent with the acceleration of the near surface wind field from the west, reflecting the diurnal increases in surface pressures west of LIT. The intensity of PBL jetogenesis is roughly correlated with the subsynoptic scale pressure rise and fall distribution which is established during the nightime period for these three case studies. The stronger the radiational cooling west of LIT, the stronger the pressure rises west of LIT, and, therefore, the stronger the pressure gradient force directed towards LIT and MEM. As can be seen in Figs. 8-11 and 12-14, the 12 hour pattern of nocturnal cooling and therefore, the 12 hour pattern of nocturnal pressure falls, controls the intensity

of low-level PBL jetogenesis which is consistent with the zonal equation of atmospheric motion (1) and the hydrostatic pressure tendency equation (2):

$$\partial u/\partial t + u\partial u/\partial x + v\partial u/\partial y + w\partial u/\partial z - fv + (1/\rho)\partial p/\partial x = 0, \qquad (1)$$

$$\frac{\partial p}{\partial t} = \int_z^{\infty} g\nabla_p \cdot \rho v \, dz + g\rho w \qquad (2)$$

These equations simply relate the increase of mean sea level pressure to density increases caused by radiational cooling. This pattern of increasing pressure can differentially accelerate an air parcel depending upon the pattern of pressure increases. Hence, due to the overnight cooling maxima located to the west of LIT, the westerly wind component increases as the pressure rises more to the west of LIT than to the east. It is apparent, however, from these figures that the magnitude of the westerly wind component comprising the core of the low-level PBL jets varies between these three case studies. The 15 August case study is the strongest because the signal of strong cooling is west of LIT, producing a strong variation in overnight pressure rises (>4 mb over northern Texas to <2 mb east of Nashville, Tennessee (BNA)). As we transition to the 16 August and 11 August case studies, the zone of maximum diurnal cooling weakens and shifts southward and eastward, which results in a reduction in the pressure rises to the west and a compensating increase in pressure rises to the south and east. These changes reduce the eastward-directed (negative) pressure gradient force in Eq. (1) over LIT within the PBL. Thus, prolonged westerly accelerations are not sustained in the 16 August case study as they are in the 15 August case study and in turn, the westerly accelerations in the 11 August case study are even weaker than in the 16 August case study. This variance reflects the fact that the cooling maxima shift eastward and southward as one compares the 15 August to

the 16 August and 11 August case studies. This reduction in the acceleration of the wind fields reflects the eastward and southward shifting in the location of the continental air mass as the synoptic scale circulation systems shift southeastward. Hence, the synoptic scale circulation acts to more substantially control the pressure gradent force within the PBL as one compares the 15 August to the 16 August and then to the 11 August case studies. This synoptic scale control of the circulation inhibits or overwhelms the mesoscale diurnal temperature changes caused by the differential nocturnal cooling, thus weakening the nocturnal pressure rise signal and the subsequent jetogenesis.

In the 24 August case study we have a very different regime in place. Here the smaller scale maxima and minima in the pressure field are overwhelmed by the synoptic scale pressure gradient force (note Figs. 7, 11, and 15). Hence, the dominance of easterly wind flow throughout the PBL reflects the horizontal pressure gradient force between the massive ridge of high pressure to the northeast over the Ohio River valley relative to the low pressure trough over the eastern Gulf of Mexico region. This relatively uniform synoptic scale northeasterly flow overwhelms the wind perturbations induced by the mesocale pressure perturbations. Mesoscale nocturnal cooling maxima, such as that over the Mississippi River valley region, are unable to make a significant perturbation in the background pressure gradient force in this case study. Hence, on this day, there is virtually no signal of organized PBL jetogenesis, thus simplifying the vertical wind shear prediction problem within the PBL. Days like this are, however, rare in the midcontinental region duringthe warm season.

2.1.4 Implications for Wind Shears and Turbulence at Memphis

We will, in this subsection of the report, compare the 5 minute synthesized data sets during the Memphis 95 deployment pushes, which were prepared by the MIT Lincoln Laboratory, to the analyses in Section 2.1.3, above. These comparisons will involve time sections of various products generated by North Carolina State University researchers from the 5 minute data sets. Figures 16-19 depict examples of these products including time

sections of cross-runway (u) wind velocity component (ms^{-1}), vertical shear of u (s^{-1}), Richardson number (Ri) (Eq. 3), and turbulent kinetic energy (TKE) (m^2s^{-2} as calculated from Eq. (4)).

$$Ri = \frac{N^2}{U_z^2} \tag{3}$$

$$TKE = \frac{1}{2} \rho \ (u'^2 + v'^2 + w'^2) \tag{4}$$

TKE was calculated by averaging the 5 minute u and v wind components over each multi-hour observational period represented in Figs. 16-19 and each 5 m vertical layer between the earth's surface and 200 m at MEM and then taking the deviations from the mean.

A comparison of the u wind component among the three westerly jetogenesis case studies, i. e., the 15, 16, and 11 August case studies, indicates a progressive weakening of the vertical wind shear zone in between the surge of westerly momentum extending down to 200 m accompanying each PBL jet and the near surface easterly flow regime as one progresses from the 15 August through the 16 and 11 August case studies. This shear zone tends to establish itself in between the 80 and 120 m levels, reflecting the interface between the westerly flow accompanying the PBL jet and the background easterlies near the earth's surface. It is one of two shear zones, with the second being established very close to the surface. It is the combination of the magnitude of the shear and the shortness of its period which produces the strongest TKE maxima. Thus, the 15 August case study far and away has the largest TKE maxima with the 11 August case study having the smallest.

The 24 August case study has a shear maximum equivalent in magnitude to the 15 August case study, however, it is relatively steady in magnitude, reflecting the quasi-steady synoptic scale northeasterly wind flow. The constancy of the shear fields reduces the

magnitude of the turbulence considerably when compared to the 15 August case study. While the sample size is small, this would indicate that a rapidly-changing nocturnal jet of large magnitude could be a very effective producer of TKE above the surface layer. Hence, if one assumes, as shown by Proctor *et al.* [1], that shear can produce potentially hazardous vortex "bounce" dynamics, that this is the type of phenomena which needs to be predicted in advance to enhance the utility of the meteorological component of AVOSS.

2.2 Development and Testing of TAPPS

While the above analyses of the meteorology during the Memphis 95 deployment was being accomplished, we were also working on the primary goal of this research project which was the development of the Terminal Area PBL Prediction System. As proposed, this problem was approached as a multi-stage issue. That is, a range of short term computational prediction systems was to be developed and tested in an effort to accomodate the level of computing power and expense which could be afforded in the operational support of the weather component of AVOSS. Figure 20 depicts the overall schematic of the four stages of TAPPS development. By the writing of this report, Stage I, which utilizes the NWS ETA prediction model described by Black [2], had been tested in a research environment, while Stage II, which employs the MASS model described by Kaplan *et al.* [3], is presently under development. Stages III-IV which employ both the MASS model and the TASS model, which is described in Proctor [4], will begin prior to the end of calender year 97.

2.2.1 Stage I of TAPPS

Stage I of TAPPS is designed to accomodate onsite environments which are computationally limited wherein the resources to support AVOSS are minimal. Thus, it is designed to be an efficient and inexpensive system but one which, because of said efficiency, necessarily lags the state-of-the-*science* in mesoscale prediction and analyses. With this goal in mind, Stage I is dependent upon acquiring simulated fields from the best

operational NWS numerical model and interpolating these fields to the region and time period of interest. In an effort to test such a concept, we attempted to acquire archived short period, i. e., three-hour, prediction fields from the current operational model employed by the NWS, i. e., the ETA model. Two versions of this model are presently being utilized in real time, i. e., a coarse mesh version employing ~48 km horizontal resolution and 50 vertical layers, i. e., the standard ETA model, and a fine mesh version, i. e., MESOETA, which employs ~29 km horizontal resolution and 50 vertical layers. After investigating the availability of archived ETA model fields, it became apparent that only 12 hourly data sets where available from both versions of the model. Even accessing these data required special permission from the Office of the Director of the National Meteorological Center. Furthermore, the standard ETA model, i. e., 48 km version output, is archived at 80 km horizontal resolution while the MESOETA model was archived at 40 km horizontal resolution. In spite of the coarseness of this information in space and time, we calculated the same products depicted in Figs. 4-7 employing standard ETA model and MESOETA model 12 hourly output and depicted these fields in Figs. 21-22 for the 15 August and 16 August case studies. Furthermore, we calculated time interpolated analogs to the 5 minute Memphis 95 data sets from the MESOETA model and calculated yields comparable to those depicted in Figs. 16-19 which are depicted in Figs. 23-26.

While these ETA model-generated data sets employ relatively coarse spatial and *very* coarse temporal resolution, there are encouraging indications that the *observed* nocturnal jets can be *simulated.* One can see proof of this when one compares the ETA and MESOETA model 12 hour simulations of potential temperature and wind velocity for the 15 and 16 August case studies valid at 1200 UTC, which are depicted in Figs. 21-22 along vertical cross sections from TOP to TLH. If one compares the 48 km ETA and 29 km MESOETA model simulations, there is a substantial increase in the magnitude of the westerly low-level PBL jet at ~300 m in the MESOETA model simulation. The wind maximum accompanying the jet is accurately located in space when compared to the

observations in Fig. 4, however, its magnitude is too weak. It is a distinct feature, however, which is not resolved in the 48 km simulation. Its simulation is likely the result of the fact that the higher resolution model resolves the cool pool of air near the surface upstream of the jet maximum as indicated by the reduction in potential temperature from ~301K in the 48 km simulation to ~298K in the 29 km simulation. Also, the higher resolution MESOETA model does a better job of resolving the inertial-advective turning of the wind generated by the increased horizontal pressure gradient force. These same trends are also apparent in the 16 August simulations, thus indicating that the use of MESOETA model products could allow the prediction of PBL nocturnal jetogenesis, albeit, the intensity of the shear accompanying the jet as well as the temporal variation of its shear is grossly underforecasted.

In spite of this encouraging information concerning the predictability of the nocturnal jetogenesis process, it is apparent from Figs. 23-26 that the lack of temporal detail in this information precludes defining the change of vertical wind shear in time. As can be seen in these figures, the constancy of the u wind component and the accompanying vertical shear fields virtually precludes any meaningful calculation of TKE, since the deviation from the mean wind velocity values at a given time can never be very large in magnitude (note Eq. (4)).

While we anticipate the operational real-time availability of higher frequency MESOETA model data sets in the future when compared to those available on archive, e. g., possibly as frequent as 3-hourly data, this still falls far short of the temporal frequency necessary to calculate meaningful TKE values, which requires data on time scales of minutes or even seconds in many cases. It is because of this limitation, among others, that much better support of AVOSS could be achieved by employing one's own more sophisticated and more temporally accessible numerical model on time scales of minutes or even seconds.

2.2.2 Stage II of TAPPS

In an effort to provide the aforementioned lack of temporal detail to TAPPS, the most efficient next step would be to employ a numerical simulation model with as much, if not more, accuracy as the MESOETA model but with much more available temporal frequency of information. The MASS model, i. e., Kaplan *et al.* [3], is now being used to formulate Stage II of TAPPS. Since this model can be run on very powerful work stations in real time, it will be more expensive and somewhat more time consuming to employ than simply accessing MESOETA model fields as was done in Stage I of TAPPS. However, it will afford a user the tremendous advantage of nearly unlimited temporal frequency in available information to be used in calculating products in support of AVOSS. This is because the time step or period of simulated time in between computations is ~10-20 seconds in MASS. Therefore, fields used in turbulence calculations could be updated on this time scale *when the model is integrated out in time on a computer or group of computers dedicated to supporting AVOSS meteorological requirements.* (Note that Fig. 20 describing the planned stages of TAPPS assumes a single processor, i. e., system A. This type of forecast capability will likely employ multiple processors running in parallel to keep ahead of the weather.)

An example of a 29 km simulation employing MASS is depicted in Fig. 27 for the 15 August case study. Analogous cross sections to those depicted in Fig. 21 are shown from three hourly simulations of the 29 km horizontal resolution MASS model run. Note that just increasing the temporal variation in model output modestly, from 12 hours to 3 hours, results in a substantial improvement in the depiction of the variation in the structure and evolution of the PBL jet. A comparison between the 3 hour simulation and 6 hour simulation shows the transition from a southeasterly near-surface wind at MEM at 3 hours to westerly near-surface flow at 6 hours (Fig. 27). This is quite consistent with the observed surge of westerly flow depicted in Fig. 16a during the 0400 UTC - 0600 UTC time period. Even though the magnitude of the westerly wind velocity is underdone in the

MASS simulation, its location in space and its timing are excellent. Furthermore, the three-hourly data indicates that the observed jetogenesis depicted in Fig. 4b is composed of multiple adjustment mechanisms, i. e., an isallobaric mechanism between 3 and 6 hours over MEM where the nocturnal cooling modifies the pressure gradient force and an inertial-advective adjustment mechanism further west over LIT near the lee slopes of the Ozark Mountains. Here, the deep well-mixed afternoon PBL and its southeasterly jet evolves into a southwesterly jet as the Coriolis force turns the flow towards the west. Thus, the nocturnal PBL jetogenesis is the sum of multiple dynamical adjustment mechanisms. Therefore, the utility of such temporal resolution is to produce considerably more realistic TKE forecasts by defining the complex dynamics. Note also that the PBL jet simulated by MASS is stronger than in the 12 hour MESOETA model simulation but still weaker than observed.

3. Work in Progress and Objectives for the Period 2/97-1/98

In the following year we plan to continue work on TAPPS Stage II and TAPPS Stage III.

3.1 TAPPS Stage II

Work will continue which involves running the MASS numerical model on the Memphis 95 case studies. Development work will focus on producing 15 km nested-grid simulations for all of these case studies and interfacing the postprocessing software, employed for calculating products from the 5 minute observed and 12 hour MESOETA model data sets (Figs. 16-19 and 23-26), with the 15 km MASS model output. Simulated 5 minute data will be employed for these diagnostic calculations from the 15 km MASS model. The MASS mesoscale model fields will be compared closely to the observations from all of the aforementioned data sets and statistical verification indices will be calculated evaluating the accuracy of the Stage II versus Stage I forecast systems. A paper will be written for the preprint volume of the upcoming AMS boundary layer symposium and

presented at the conference in Vancouver, British Columbia. Also, a journal article detailing nocturnal jetogenesis dynamics and predictability will be submitted to the Journal of Applied Meteorology.

3.2 TAPPS Stage III

Work will begin to initialize the TASS model from 15 km nested-grid MASS model output. This will require modifying the TASS preprocessor to handle horizontally varying initial fields. These new initial conditions will be tested in a one-way boundary condition version of TASS. The new boundary conditions being developed now for TASS will be tested by using lateral information communicated from the MASS 15 km simulations to TASS. Work will also begin on modifying TASS to a terrain-following coordinate system.

3.3 Incorporation of Operational Profiler Data

In addition to model testing and development, we will be making an effort to improve the pressure and temperature data sets which could be incorporated into the initial state of TAPPS. A technique published in Cram *et al.* [5] and tested in Adams *et al.* [6] which derives mass information from wind data will be tested on the 15 and 16 August 1995 case studies. This technique employs wind profiler data from the two-dimensional wind velocity divergence equation to produce consistent pressure and temperature fields at many vertical levels in the atmosphere. This information could help to initialize TAPPS over the midcontinent region where wind profiler data is much more plentiful in space and time than rawinsonde data. An innovation which must be tested, however, is the modification of the technique to employ profiler-derived winds within the PBL. This task will be undertaken in an effort to enhance the initial data sets for use in TAPPS, particularly when TAPPS is initialized at asynoptic time periods, i. e., at times other than 0000 UTC or 1200 UTC.

4. References

[1] Proctor, F. H., Hinton, D. A., Han, J., Schowalter, D. G., and Lin, Y.-L., 1996. Two-dimensional wake vortex simulations in the atmosphere: Preliminary sensitivity studies. AIAA Paper 97-0056.

[2] Black, T. L., 1994: The new NMC mesoscale ETA model: Description and forecast examples. *Wea. Forecasting*, **9**, 265-278.

[3] Kaplan, M. L., S. E. Koch, Y.-L. Lin, R. P. Weglarz, and R. A. Rozumalski, 1997: Numerical simulations of a gravity wave event over CCOPE. Part I: The role of geostrophic adjustment in mesoscale jetlet formation. In press, *Mon. Wea. Rev.*

[4] Proctor, F. H., 1987. The Terminal Area Simulation System Volume I: Theoretical Formulation. NASA Contractor Report 4046 DOT/FAA/PM-86/50,I.

[5] Cram, J. M., M. L. Kaplan, C. A. Mattocks, and J. W. Zack, 1991: The use and analysis of profiler winds to derive mesoscale height and temperature fields: Simulation and real data experiments. *Mon. Wea. Rev.*, **119**, 1040-1056.

[6] Adams, M. E., S. Businger, M. L. Kaplan, and S. E. Koch, 1997: Extraction of geopotential height and temperature structure from observed profiler winds over the central plains during STORM-FEST. Submitted to *J. Appl. Meteor.* for publication.

5. Papers submitted in Calender Year 1996

Kaplan, M. L., R. P. Weglarz, D. W. Hamilton, and Y.-L. Lin, 1997: Synergistic interaction between a Great Plains nocturnal low-level jet and the mass adjustments accompanying a subtropical jet streak. Submitted for Oral Presentation at the *12th Symposium on Boundary Layers and Turbulence*, 28 July-1 August, Vancouver, British Columbia, Canada.

6. List of Figures

1. a) Isotherms of mean January temperatures reduced to sea level for the United States. b) Isotherms of mean July temperatures reduced to sea level for the United States. (Both maps after C.F. Brooks, A. O. Connor, and others, *Climate of North America*)

2. Sunshine distribution over the United States in per cent of possible sunshine (according to Kincer).

3. Surface and rawinsonde stations utilized for the dynamical analyses of the meteorology during the Memphis 95 deployment. Thick dashed lines represent the location of vertical cross sections employed to analyze rawinsonde and numerical model output.

4. Vertical cross sections from Topeka, Kansas (TOP) to Tallahassee, Florida (TLH) of observed rawinsonde-derived potential temperature (solid in K) and wind velocity (dotted in ms^{-1}) valid at a) 0000 UTC and b) 1200 UTC 15 August 1995. Wind barbs at each rawinsonde location represent observed 50 mb vertically interpolated wind direction and magnitude with full barb=10 ms^{-1}, half barb=2.5 ms^{-1}, and no barb=0 ms^{-1}.

5. Same as Figure 4 for 16 August 1995.

6. Same as Figure 4 for 11 August 1995.

7. Same as Figure 4 for 24 August 1995.

8. Observed surface temperature change (negative dashed in C) for the period from 0000 UTC - 1200 UTC 15 August 1995.

9. Same as Figure 8 for 16 August 1995.

10. Same as Figure 8 for 11 August 1995.

11. Same as Figure 8 for 24 August 1995.

12. Observed mean sea level pressure change (positive solid in mb) for the period from 0000 UTC - 1200 UTC 15 August 1995.

13. Same as Figure 12 for 16 August 1995.

14. Same as Figure 12 for 11 August 1995.

15. Same as Figure 12 for 24 August 1995.

16. Time section of observed 5 minute special data sets at MEM including a) u wind velocity component (solid positive in ms^{-1}), b) vertical shear of u wind velocity component (positive solid in s^{-1}), and c) Richardson number (shaded less than .25) and turbulent kinetic energy (solid in m^2s^{-2}) valid from ~0330 UTC 15 August -~0600 UTC 15 August 1995.

17. Same as Figure 16 for ~0300 UTC - ~0600 UTC 16 August 1995.

18. Same as Figure 16 for ~0400 UTC - ~0600 UTC 11 August 1995.

19. Same as Figure 16 for ~0330 UTC - ~0630 UTC 24 August 1995.

20. Schematic depicting Stages I-IV timeline for TAPPS.

21. 12 hour simulated vertical cross section from TOP - TLH of potential temperature (solid in C), isotachs (dashed in ms^{-1}), and wind vectors (as in Figure 4) valid at 1200 UTC 15 August 1995 from the a) 48 km ETA model and b) 29 km MESOETA model.

22. Same as Figure 21 for 16 August 1995.

23. MESOETA 12 hour simulation of a) u wind velocity component (solid positive in ms^{-1}) and b) vertical shear of the u wind velocity component (positive solid in s^{-1}) interpolated to the time period from ~0330 UTC 15 August - ~0600 UTC 15 August 1995.

24. Same as Figure 23 for ~0300 UTC - ~0600 UTC 16 August 1995.

25. Same as Figure 23 for ~0400 UTC - ~0600 UTC 11 August 1995.

26. Same as Figure 23 for ~0330 UTC - ~0630 UTC 24 August 1995.

27. Same as Figure 21 for the MASS model simulations valid 3-hourly at a) 0300 UTC, b) 0600 UTC, c) 0900 UTC, and d) 1200 UTC 15 August 1995.

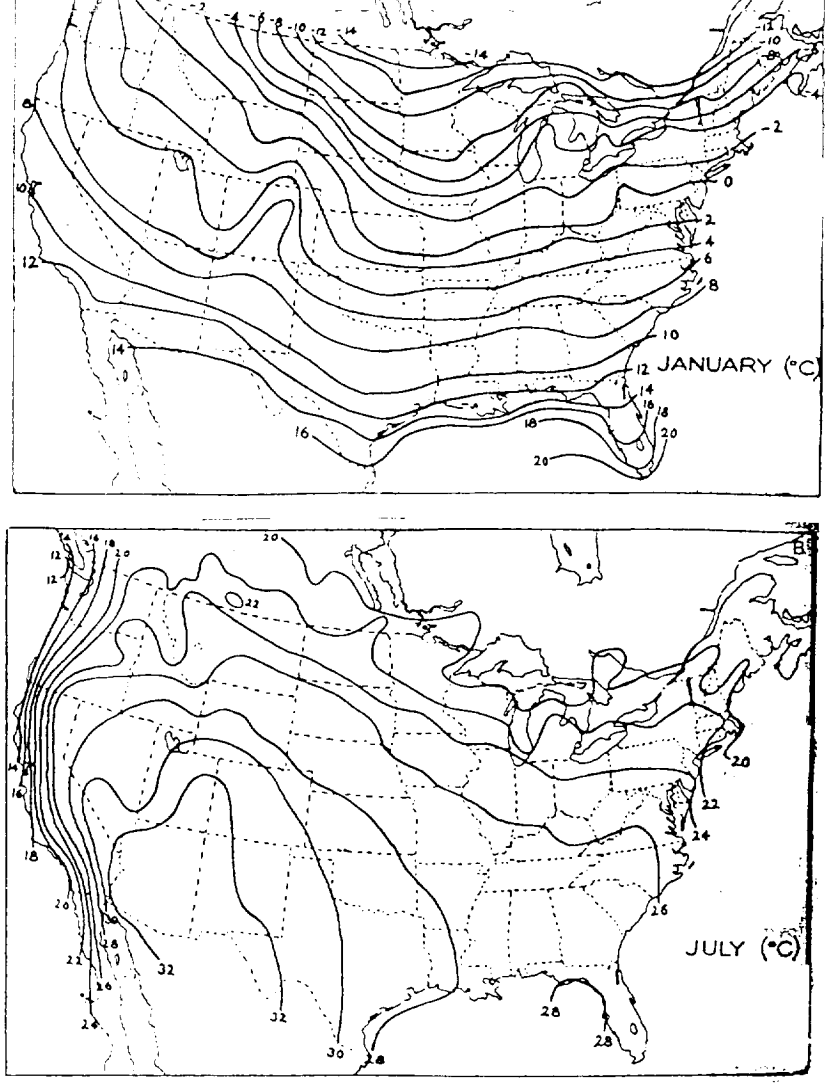

1. a) Isotherms of mean January temperatures reduced to sea level for the United States. b) Isotherms of mean July temperatures reduced to sea level for the United States. (Both maps after C.F. Brooks, A. O. Connor, and others, Climate of North America.)

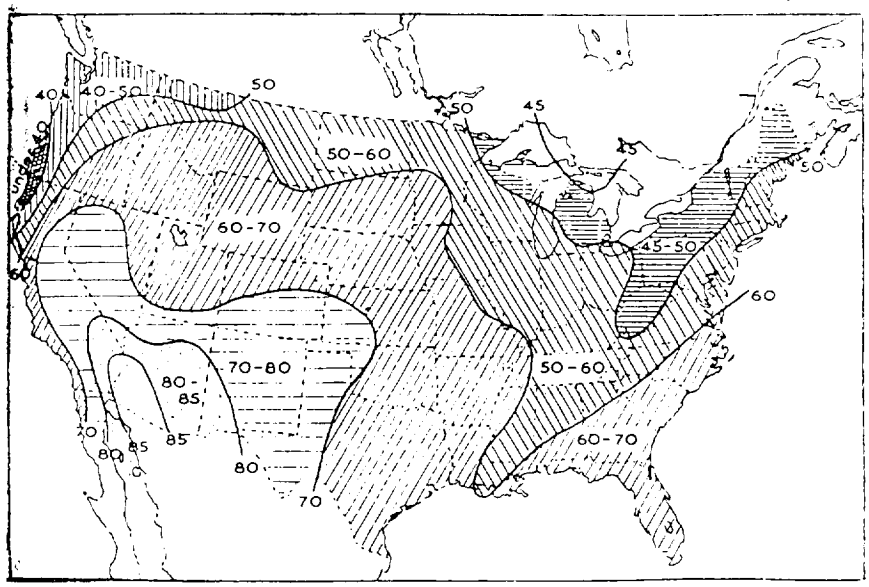

2. Sunshine distribution over the United States in per cent of possible sunshine (according to Kincer).

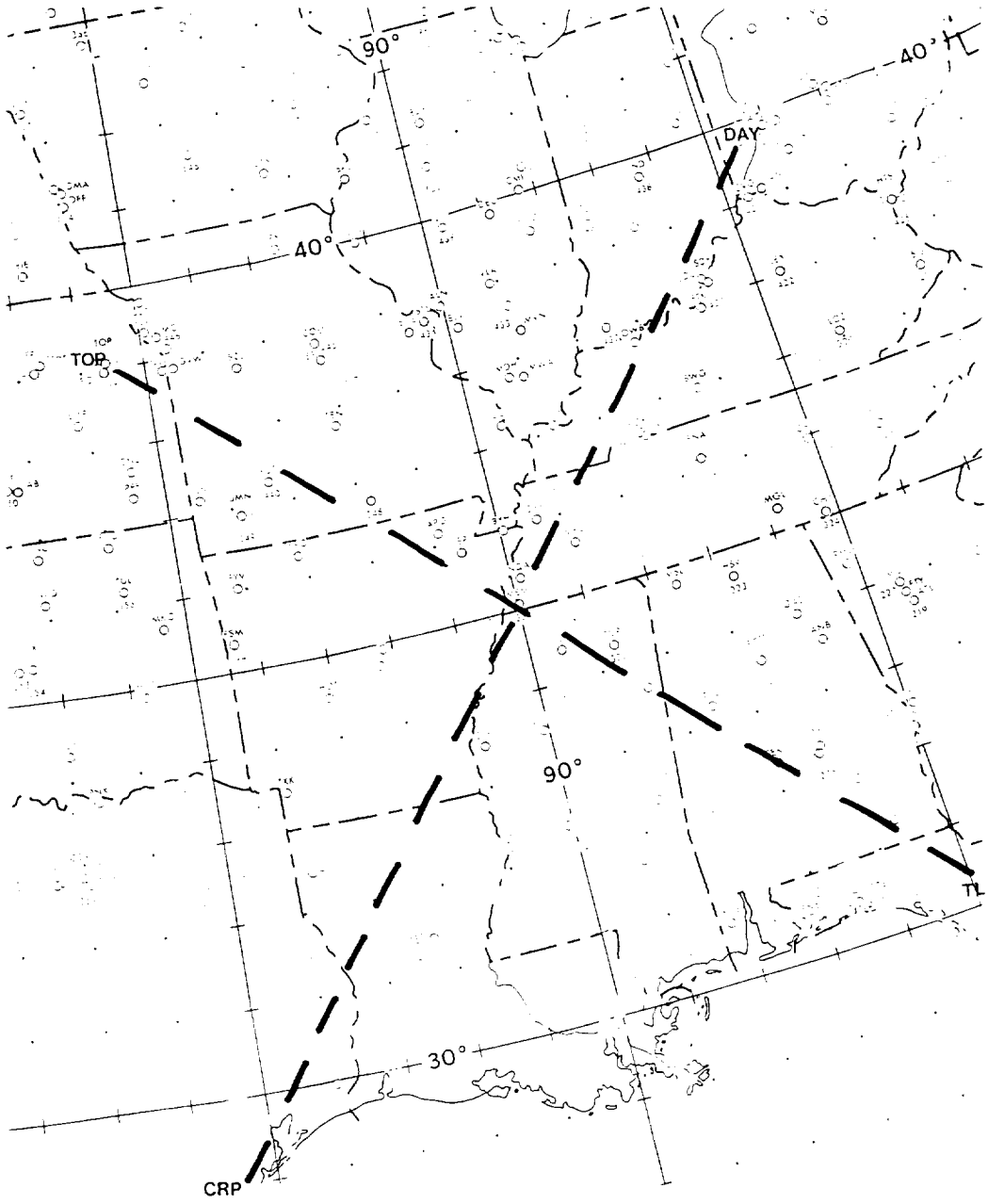

3. Surface and rawinsonde stations utilized for the dynamical analyses of the meteorology during the Memphis 95 deployment. Thick dashed lines represent the location of vertical cross sections employed to analyze rawinsonde and numerical model output.

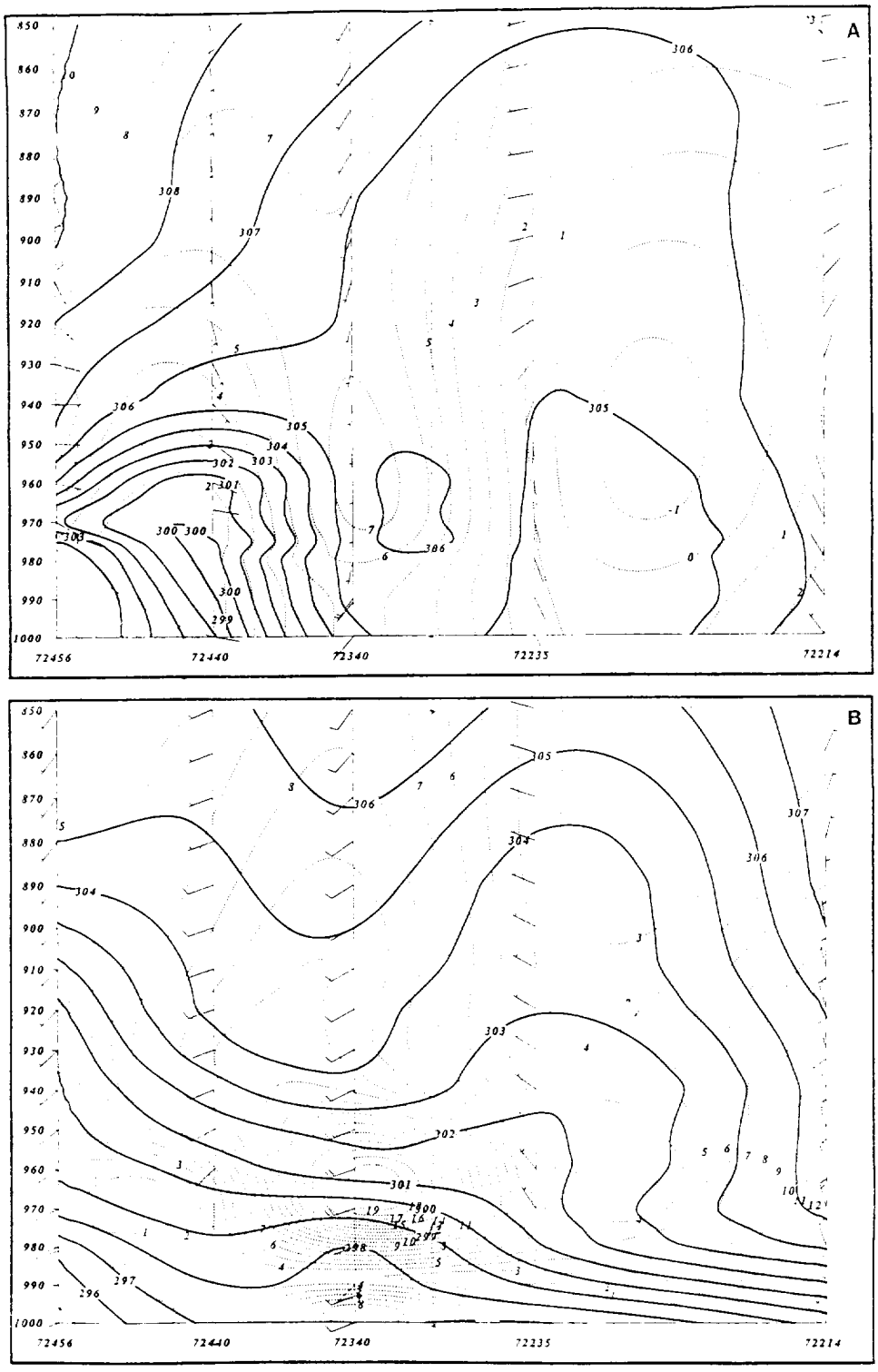

4. Vertical cross sections from Topeka, Kansas (TOP) to Tallahassee, Florida (TLH) of observed rawinsonde-derived potential temperature (solid in K) and wind velocity (dotted in ms-1) valid at a) 0000 UTC and b) 1200 UTC 15 August 1995. Wind barbs at each rawinsonde location represent observed 50 mb vertically interpolated wind direction and magnitude with full barb=10 ms^{-1}, half barb=2.5 ms^{-1}, and no barb=0 ms^{-1}.

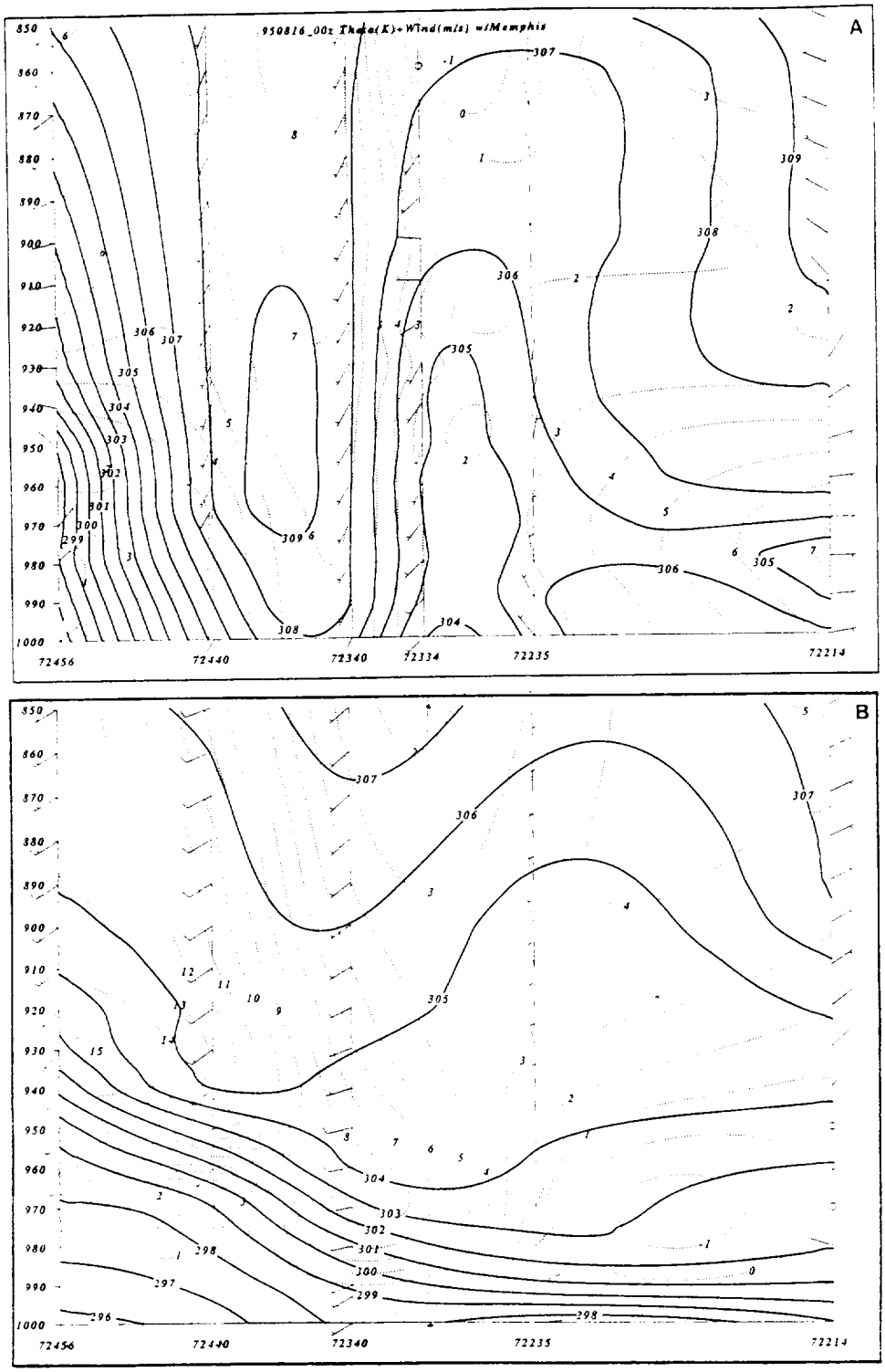

5. Same as Figure 4 for 16 August 1995.

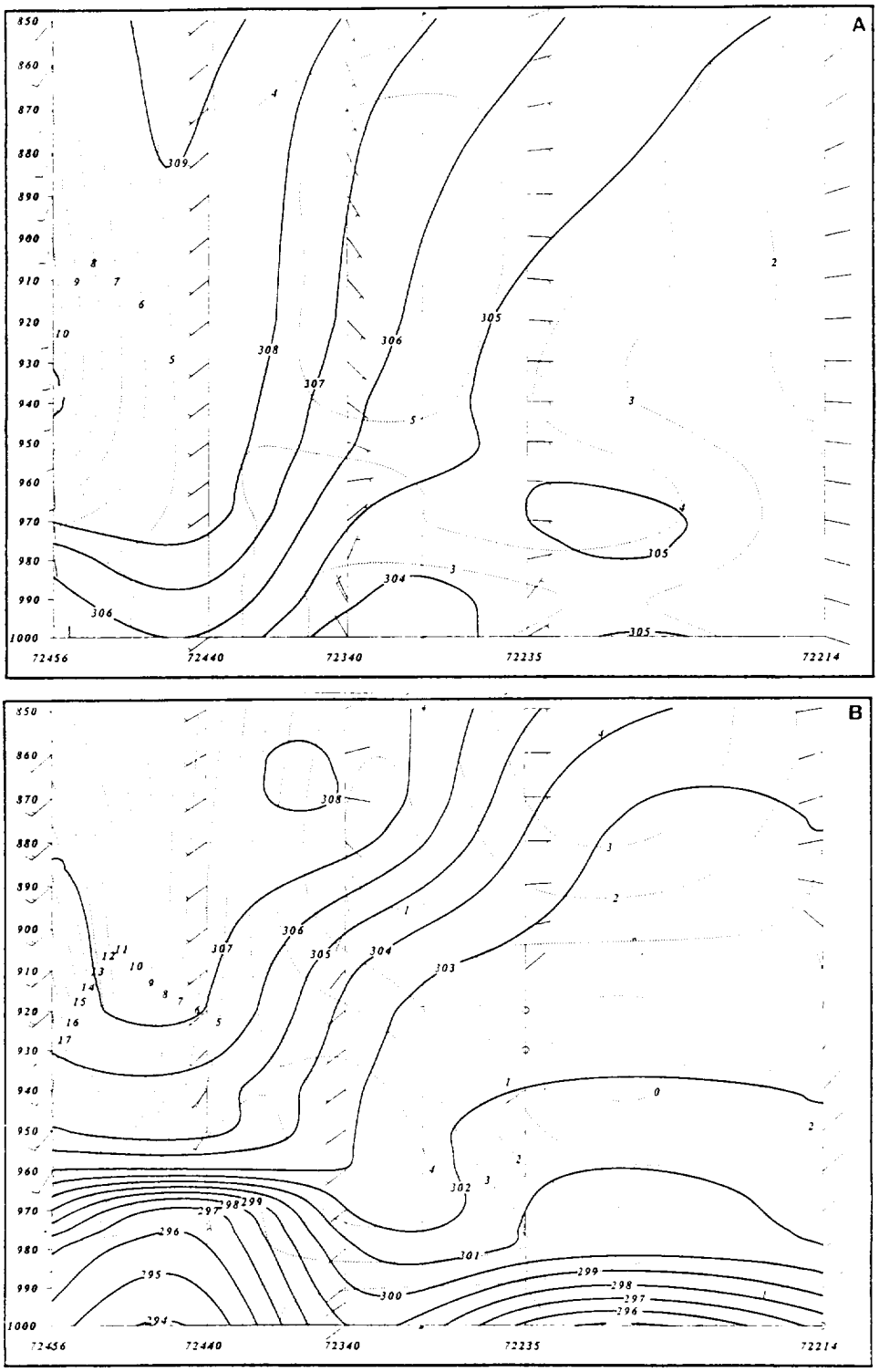

6. Same as Figure 4 for 11 August 1995.

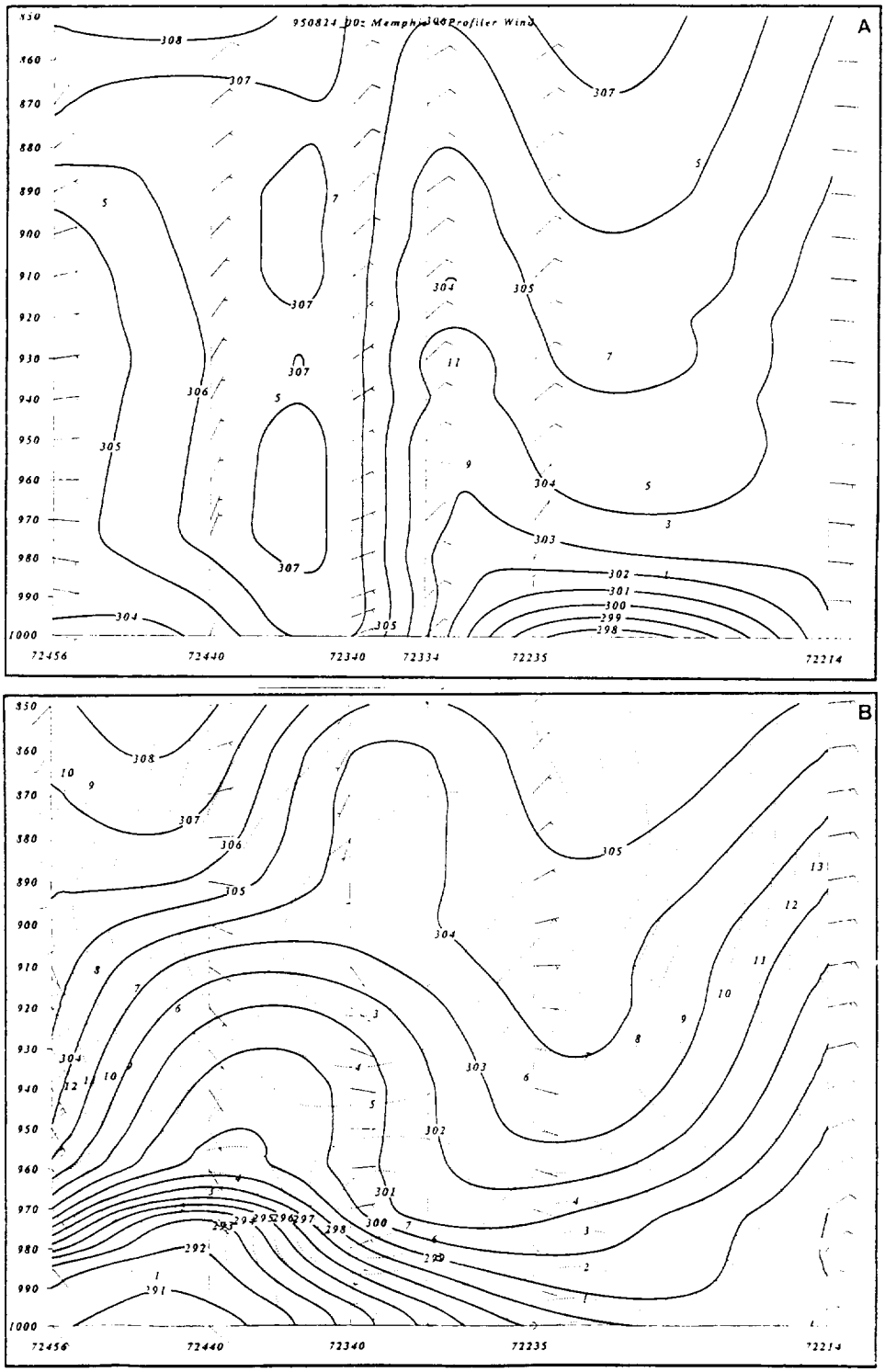

7. Same as Figure 4 for 24 August 1995.

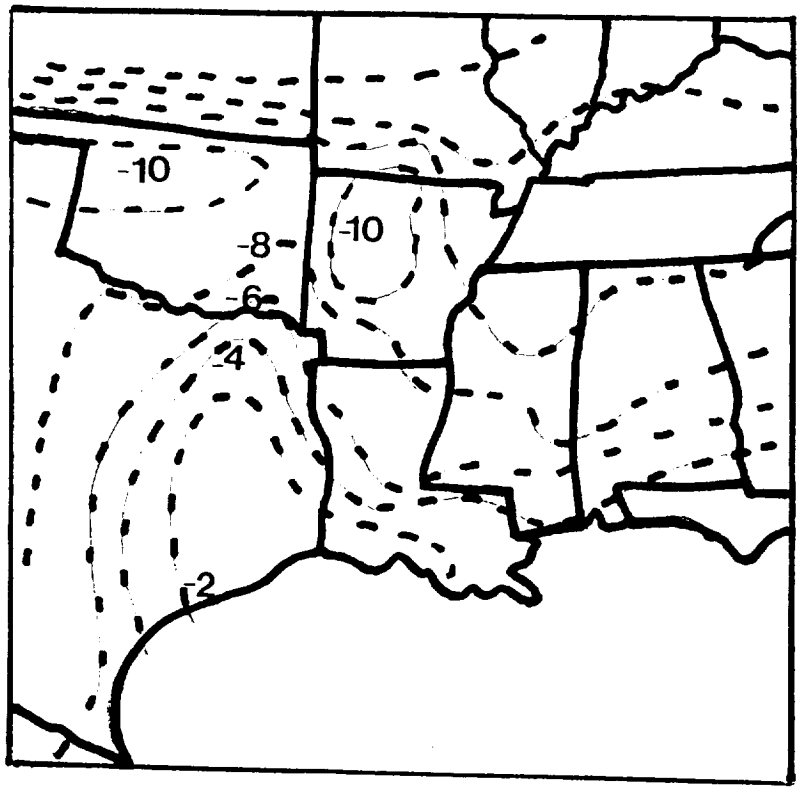

8. Observed surface temperature change (negative dashed in C) for the period from 0000 UTC - 1200 UTC 15 August 1995.

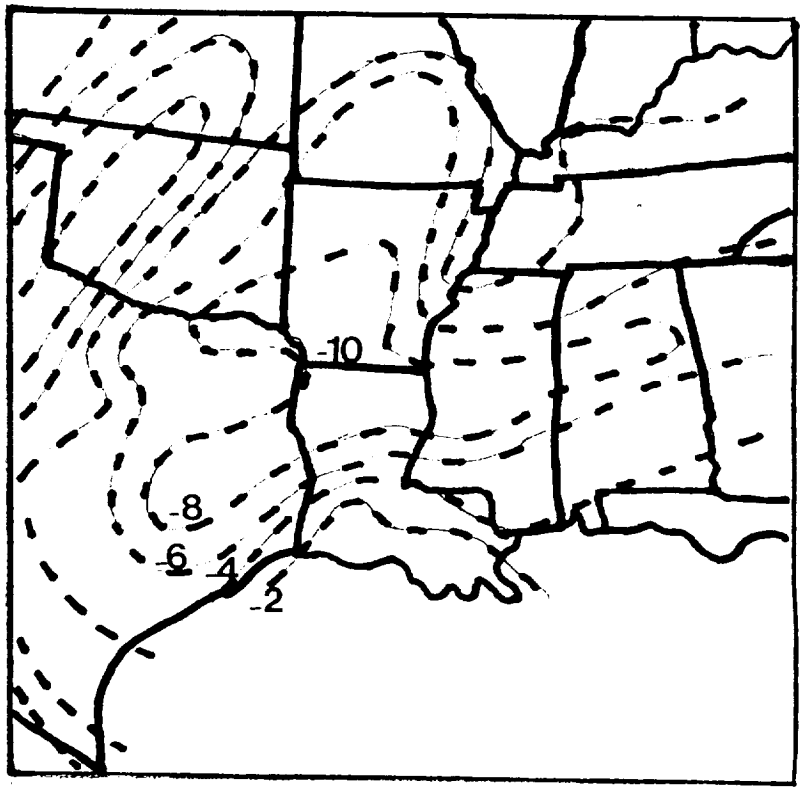

9. Same as Figure 8 for 16 August 1995.

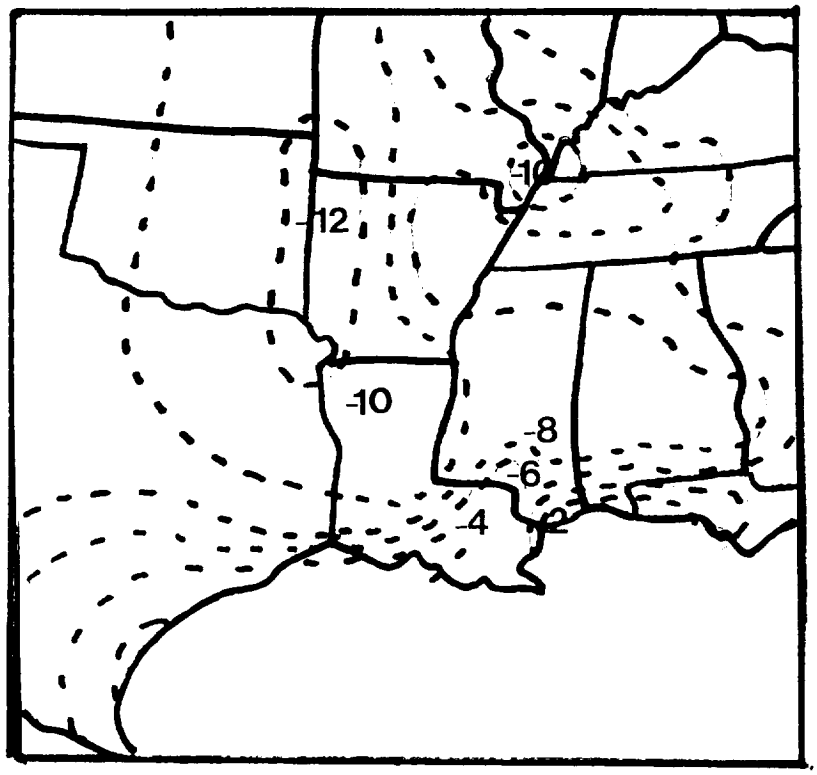

10. Same as Figure 8 for 11 August 1995.

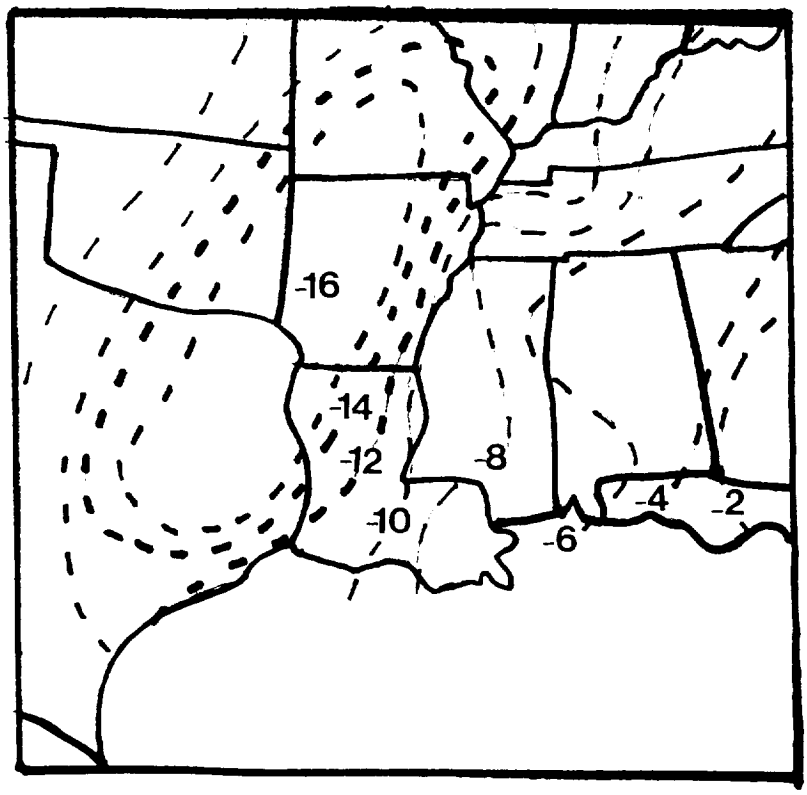

11. Same as Figure 8 for 24 August 1995.

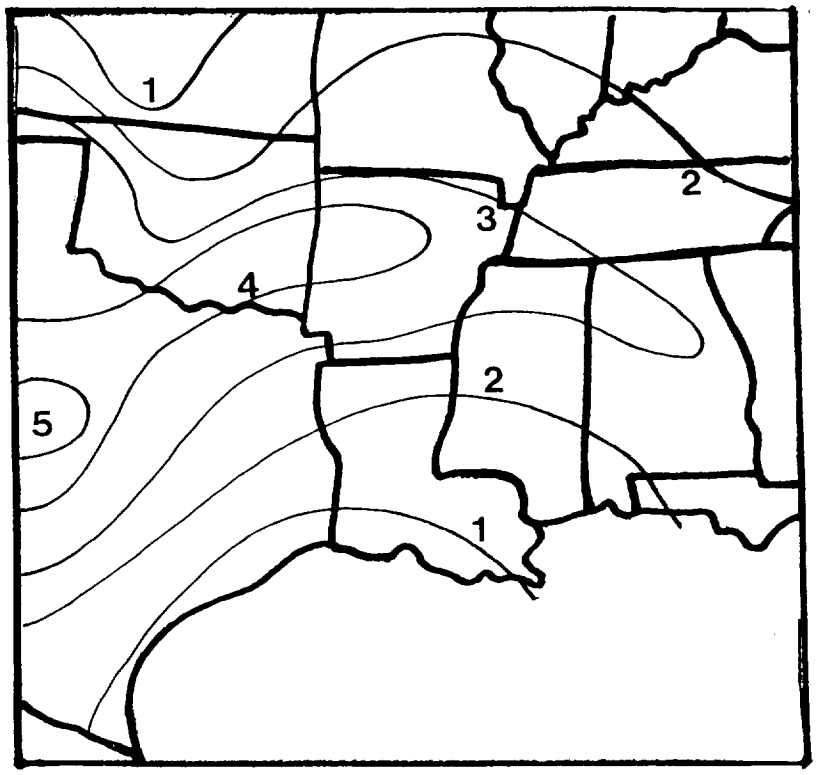

12. Observed mean sea level pressure change (positive solid in mb) for the period from 0000 UTC - 1200 UTC 15 August 1995.

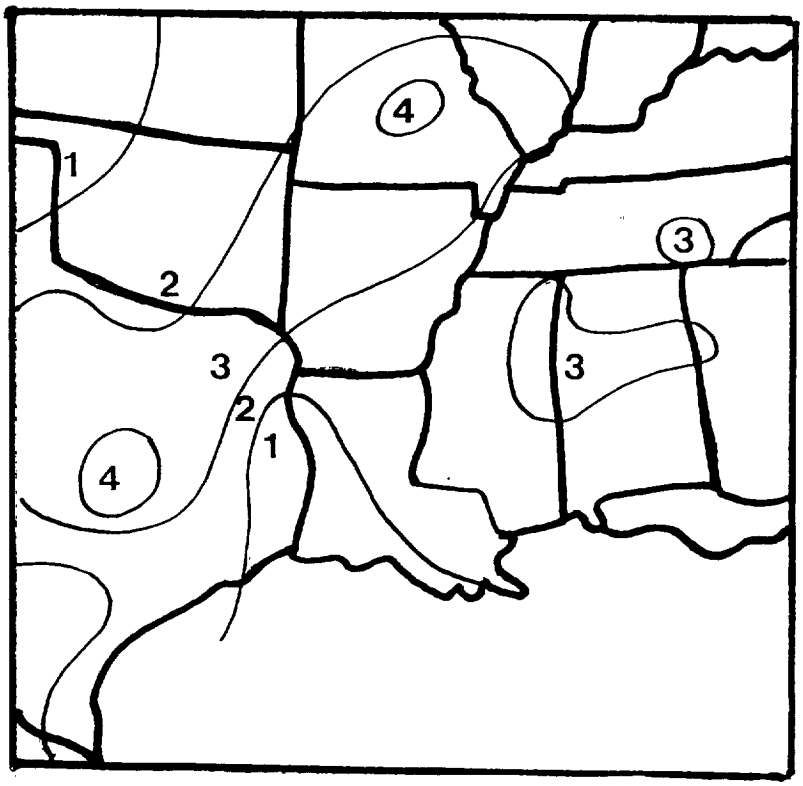

13. Same as Figure 12 for 16 August 1995.

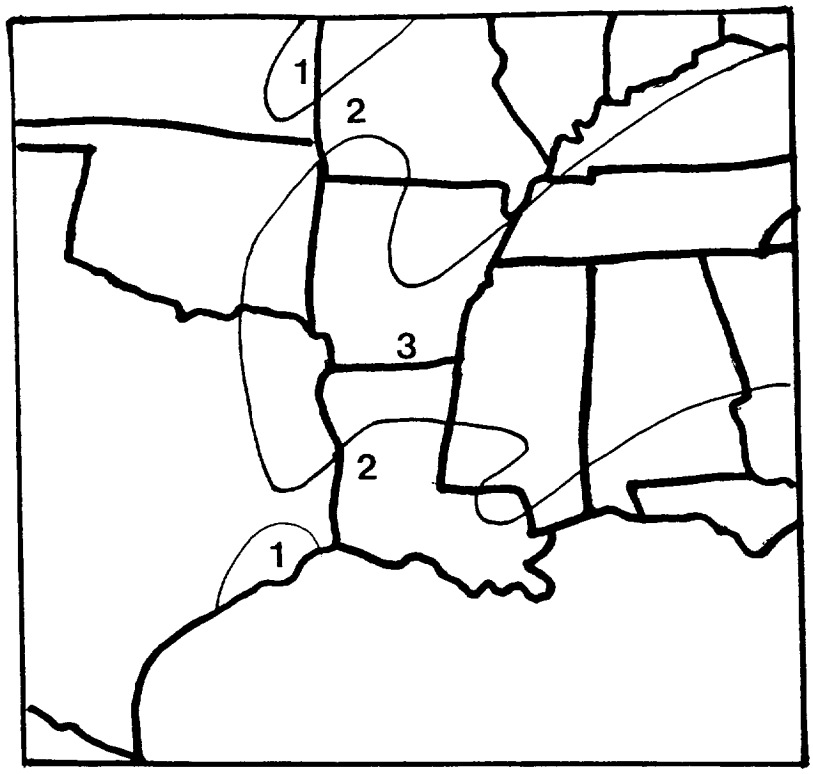

14. Same as Figure 12 for 11 August 1995.

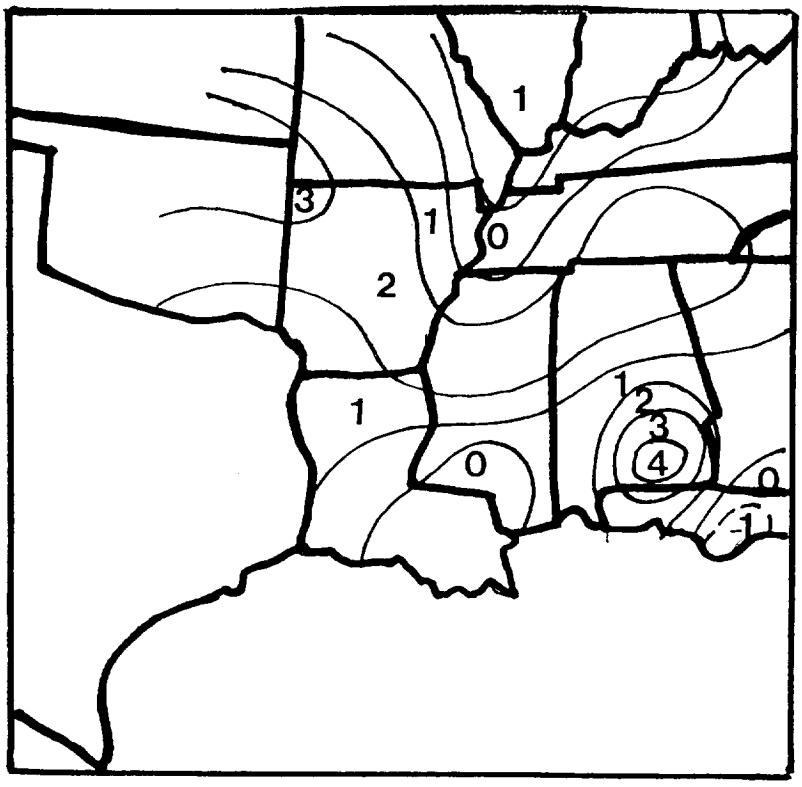

15. Same as Figure 12 for 24 August 1995.

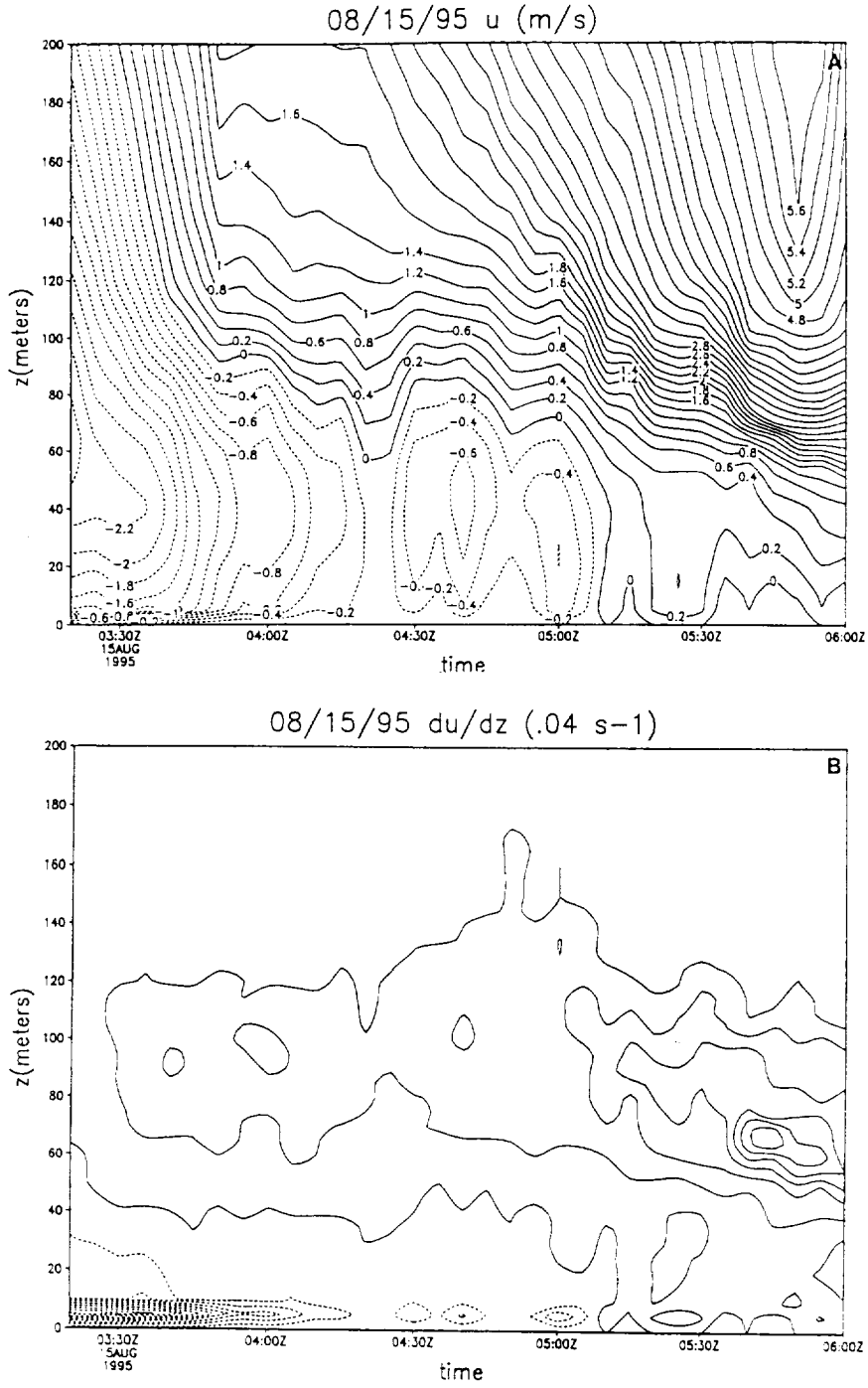

16. Time section of observed 5 minute special data sets at MEM including a) u wind velocity component (solid positive in ms^{-1}), b) vertical shear of u wind velocity component (positive solid in s^{-1}), and c) Richardson number (shaded less than .25) and turbulent kinetic energy (solid in m^2s^{-2}) valid from ~0330 UTC 15 August -~0600 UTC 15 August 1995.

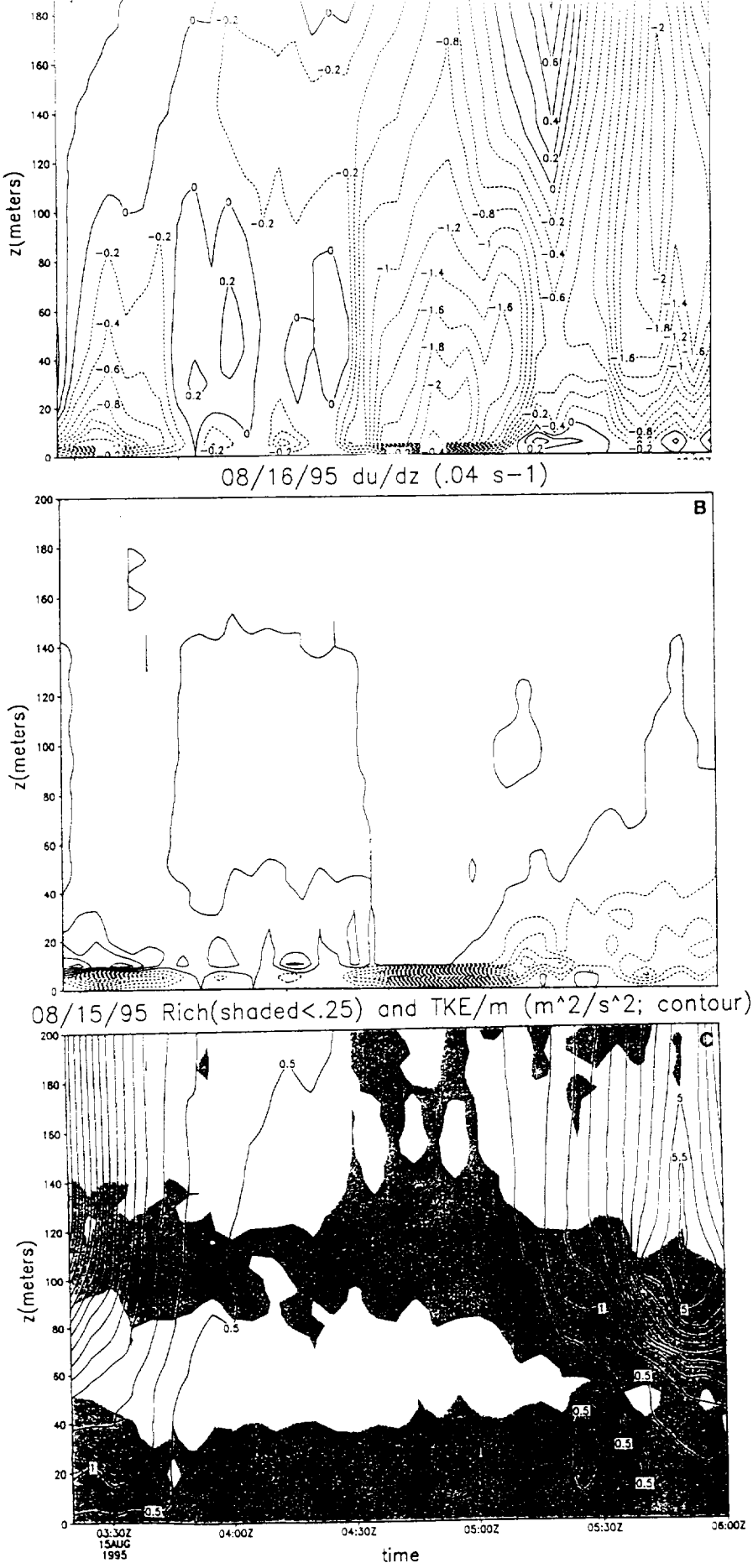

17. Same as Figure 16 for ~0300 UTC - ~0600 UTC 16 August 1995.

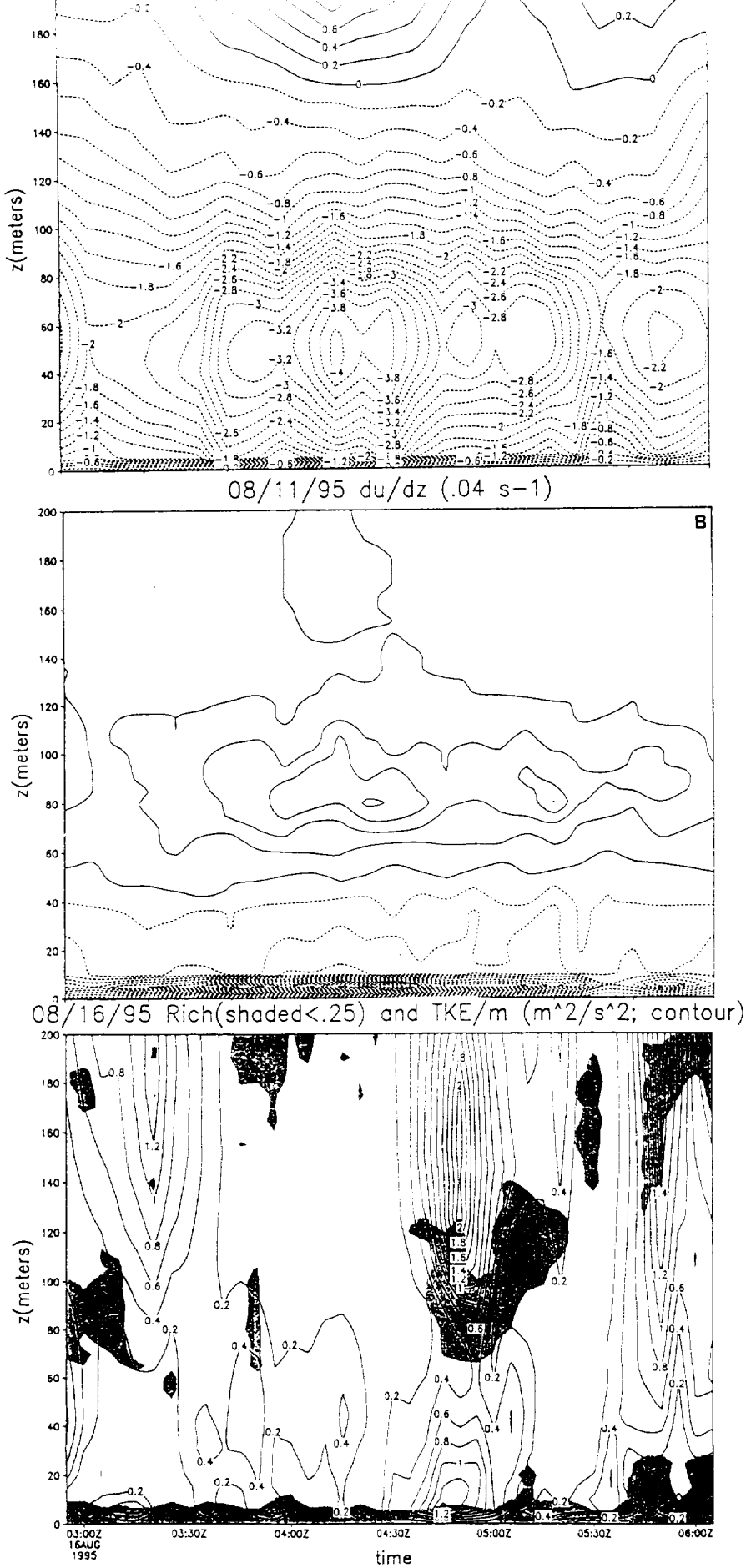

18. Same as Figure 16 for ~0400 UTC - ~0600 UTC 11 August 1995.

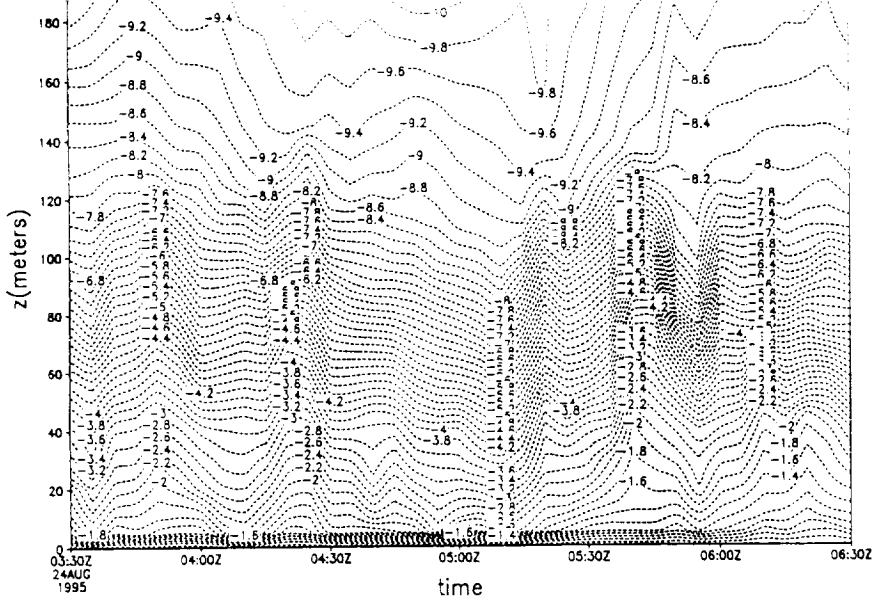

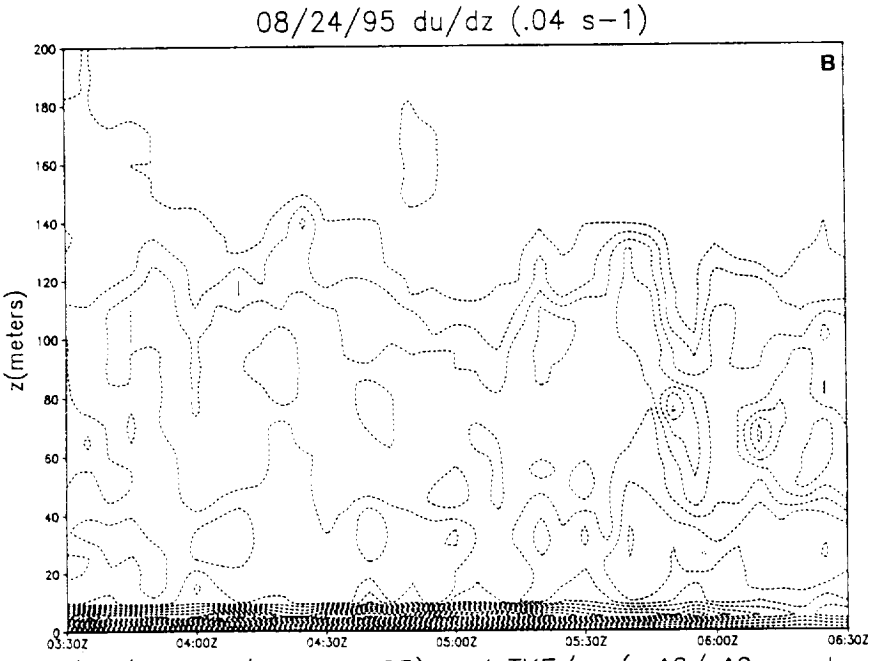

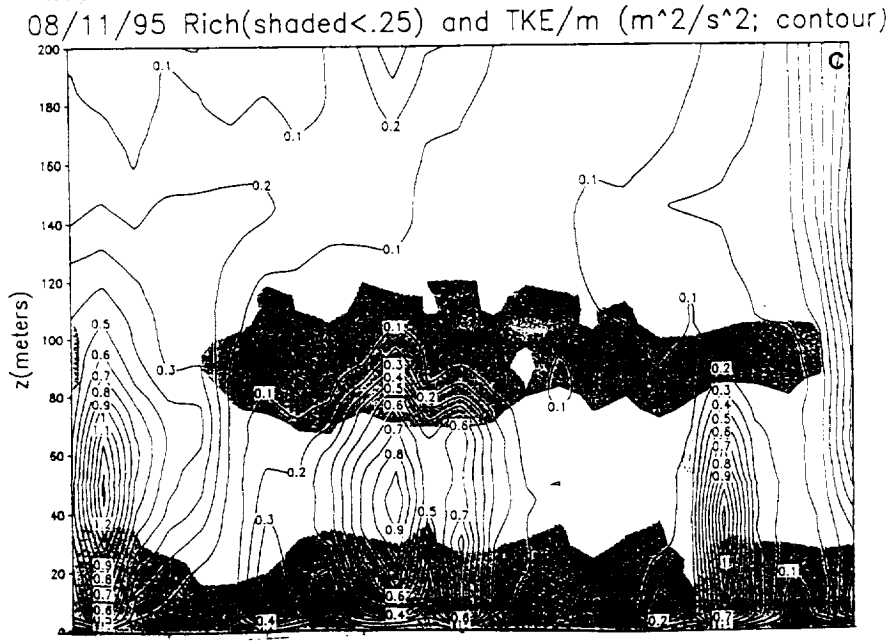

19. Same as Figure 16 for ~0330 UTC - ~0630 UTC 24 August 1995.

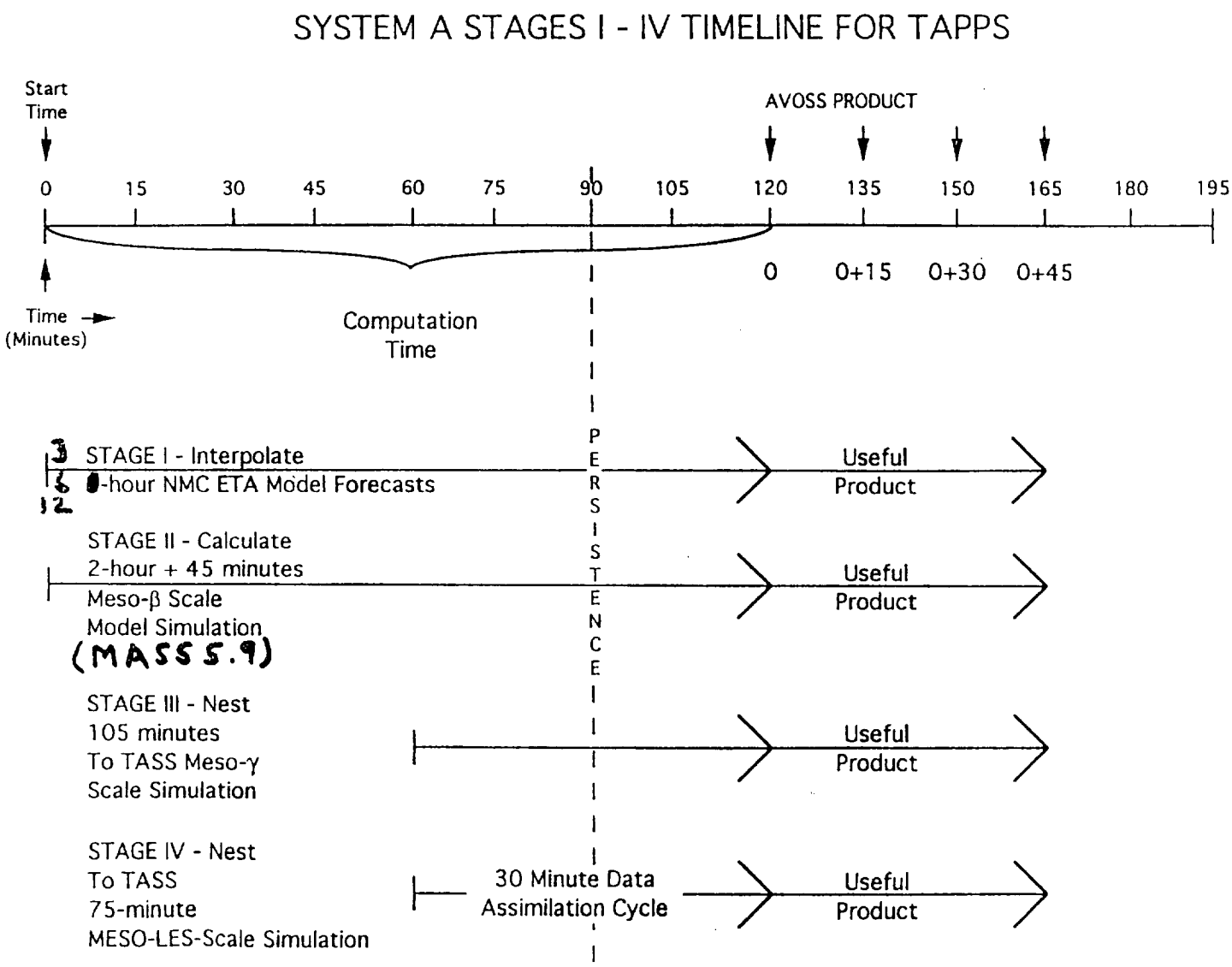

20. Schematic depicting Stages I-IV timeline for TAPPS.

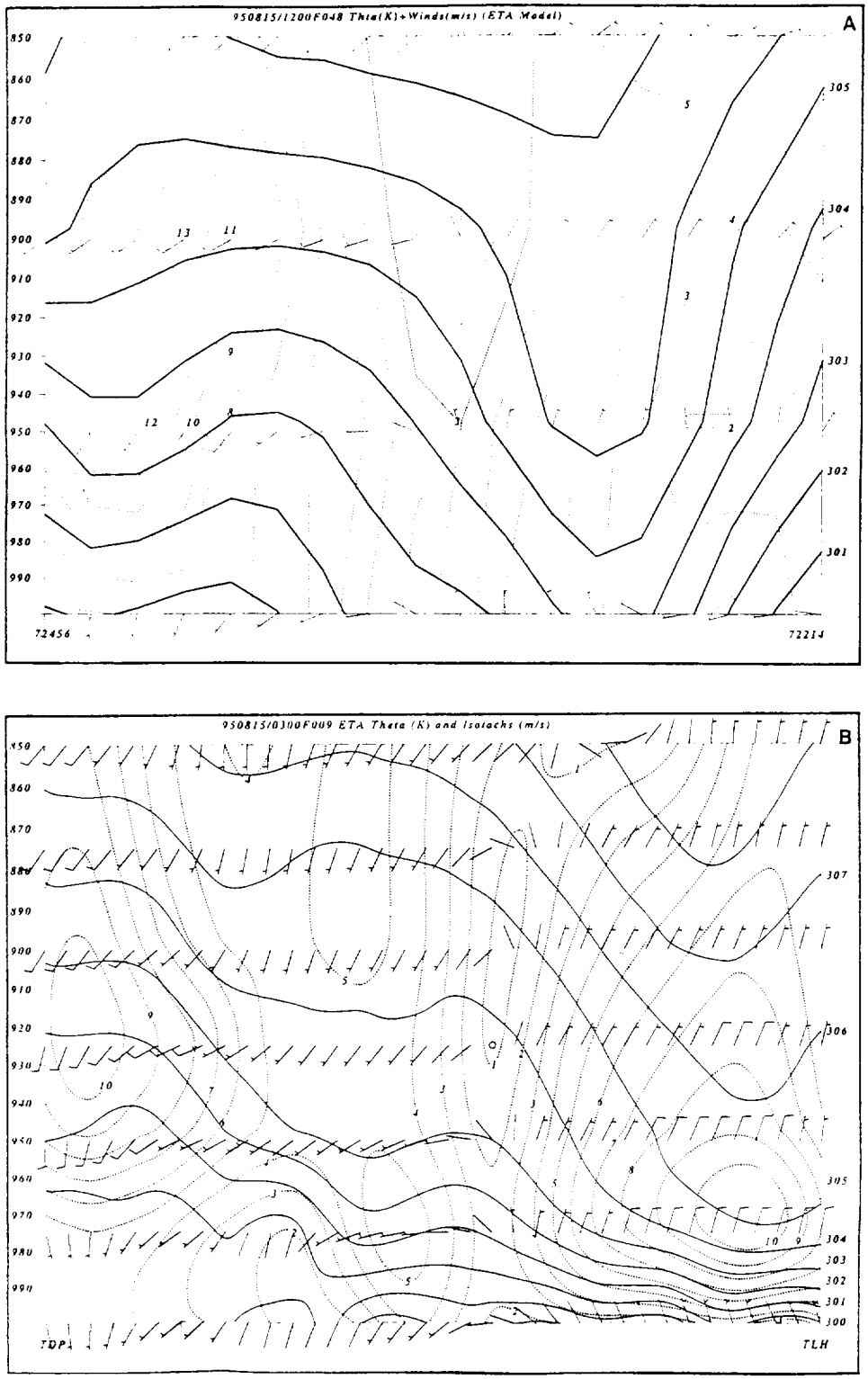

21. 12 hour simulated vertical cross section from TOP - TLH of potential temperature (solid in C), isotachs (dashed in ms^{-1}), and wind vectors (as in Figure 4) valid at 1200 UTC 15 August 1995 from the a) 48 km ETA model and b) 29 km MESOETA model.

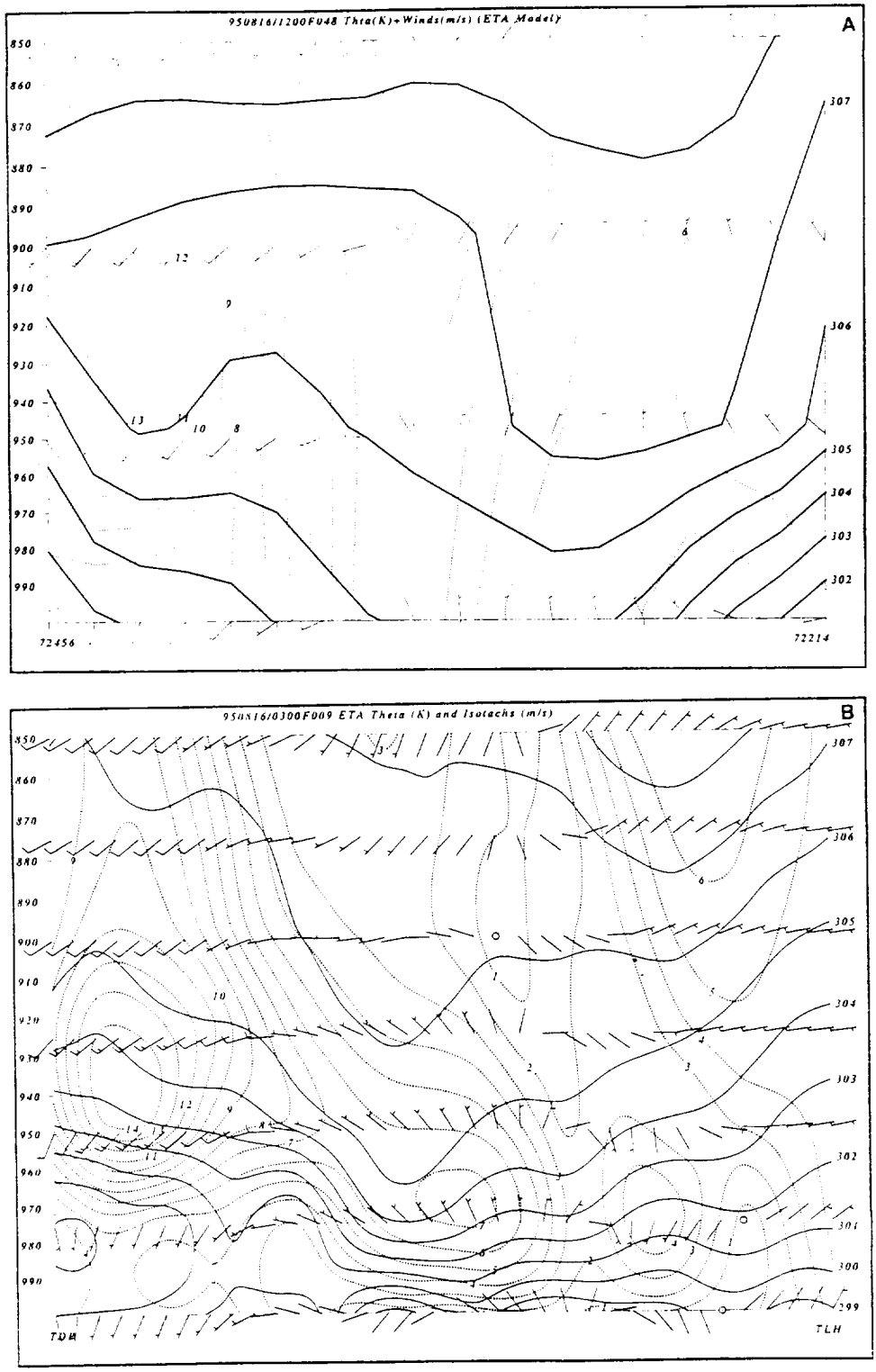

22. Same as Figure 21 for 16 August 1995.

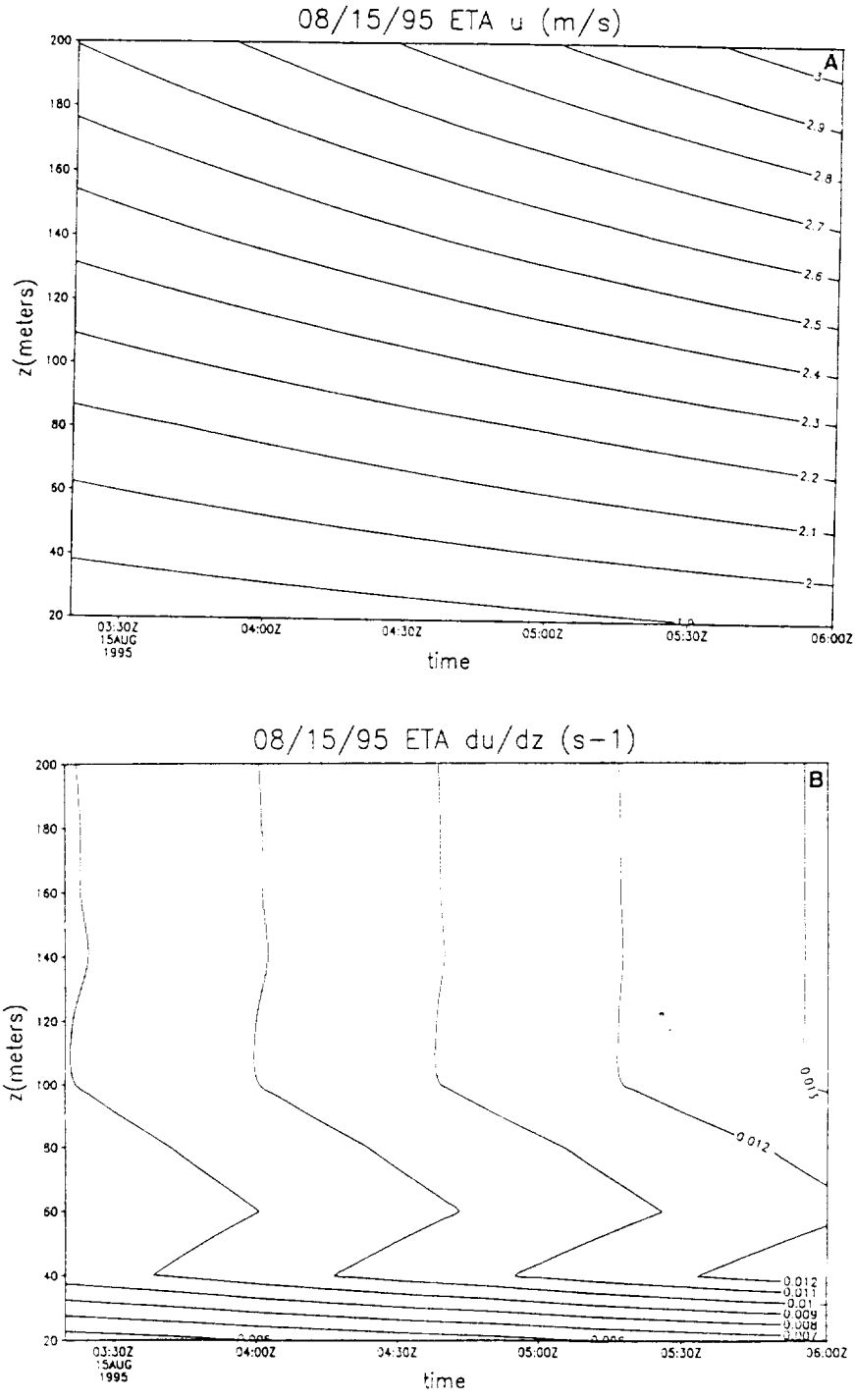

23. MESOETA 12 hour simulation of a) u wind velocity component (solid positive in ms^{-1}) and b) vertical shear of the u wind velocity component (positive solid in s^{-1}) interpolated to the time period from ~0330 UTC 15 August - ~0600 UTC 15 August 1995.

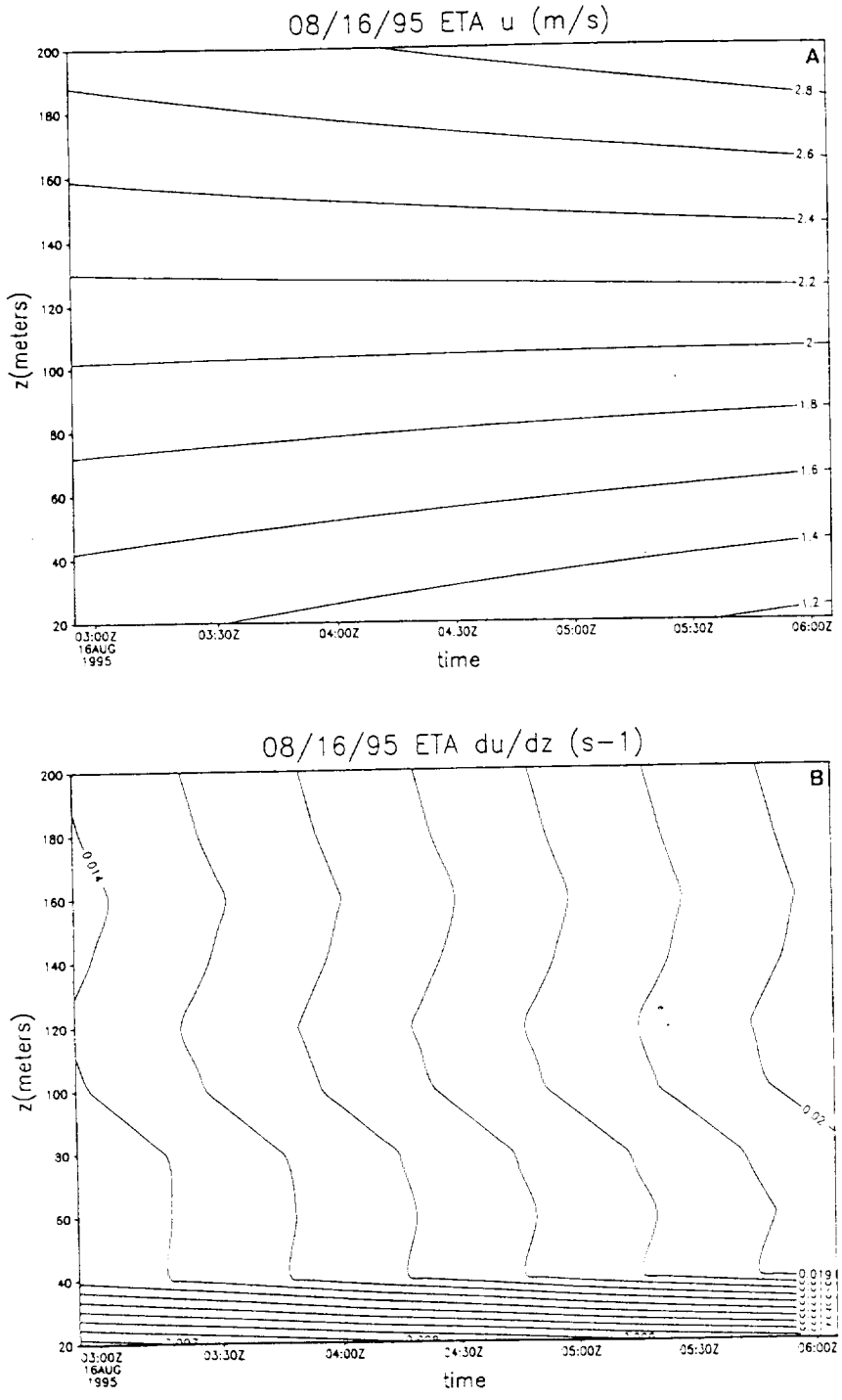

24. Same as Figure 23 for ~0300 UTC - ~0600 UTC 16 August 1995.

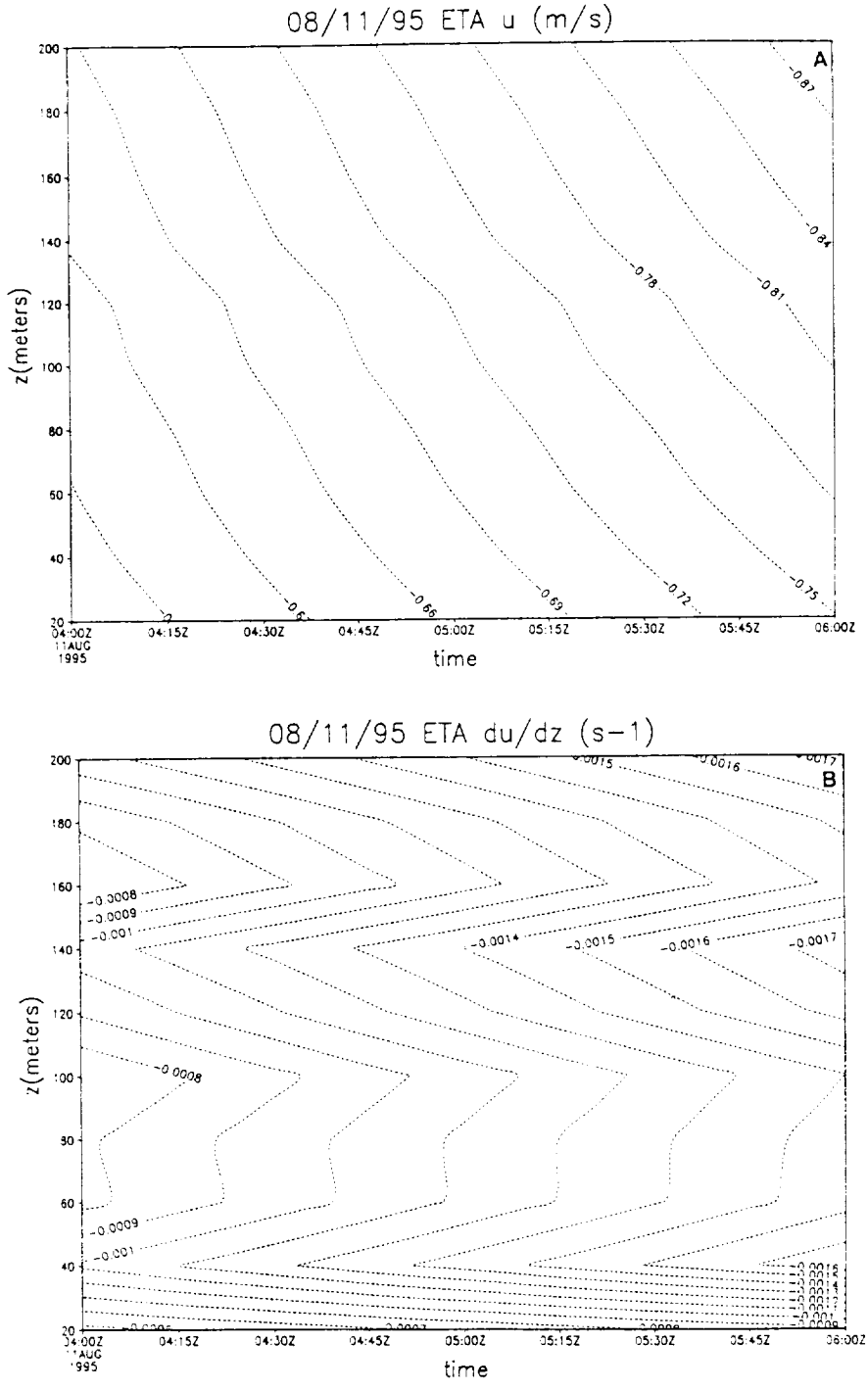

25. Same as Figure 23 for ~0400 UTC - ~0600 UTC 11 August 1995.

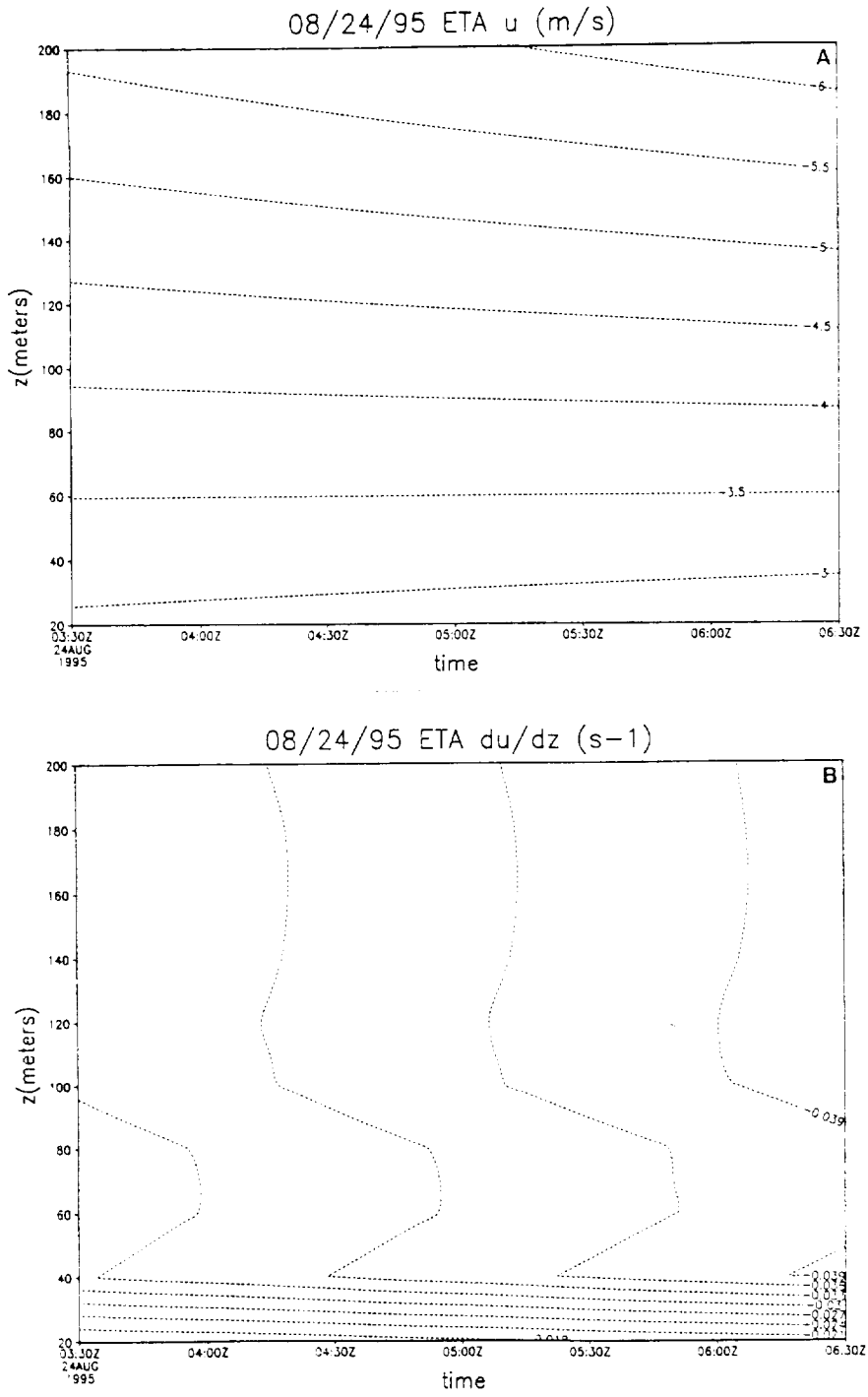

26. Same as Figure 23 for ~0330 UTC - ~0630 UTC 24 August 1995.

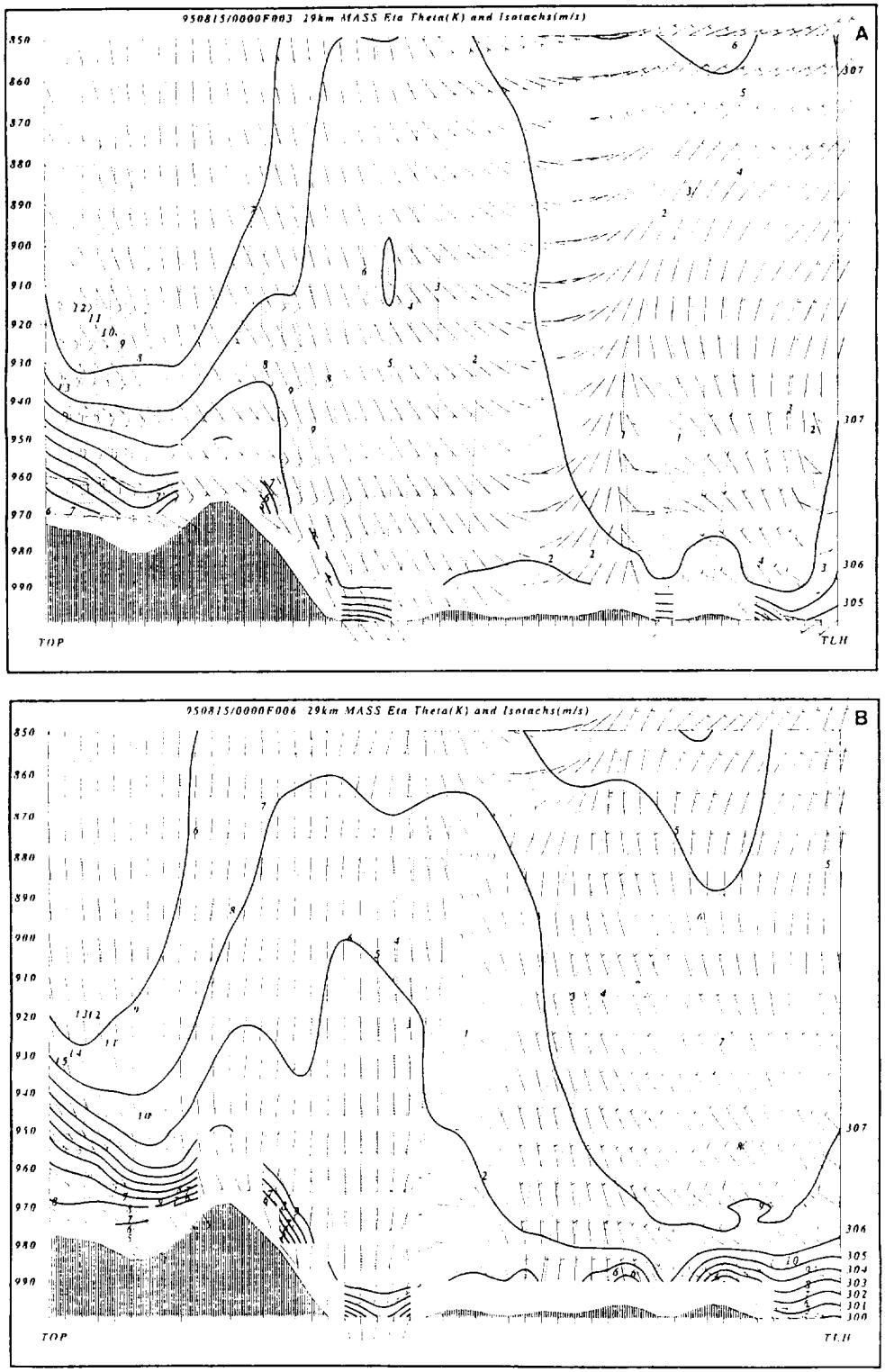

27. Same as Figure 21 for the MASS model simulations valid 3-hourly at a) 0300 UTC, b) 0600 UTC, c) 0900 UTC, and d) 1200 UTC 15 August 1995.

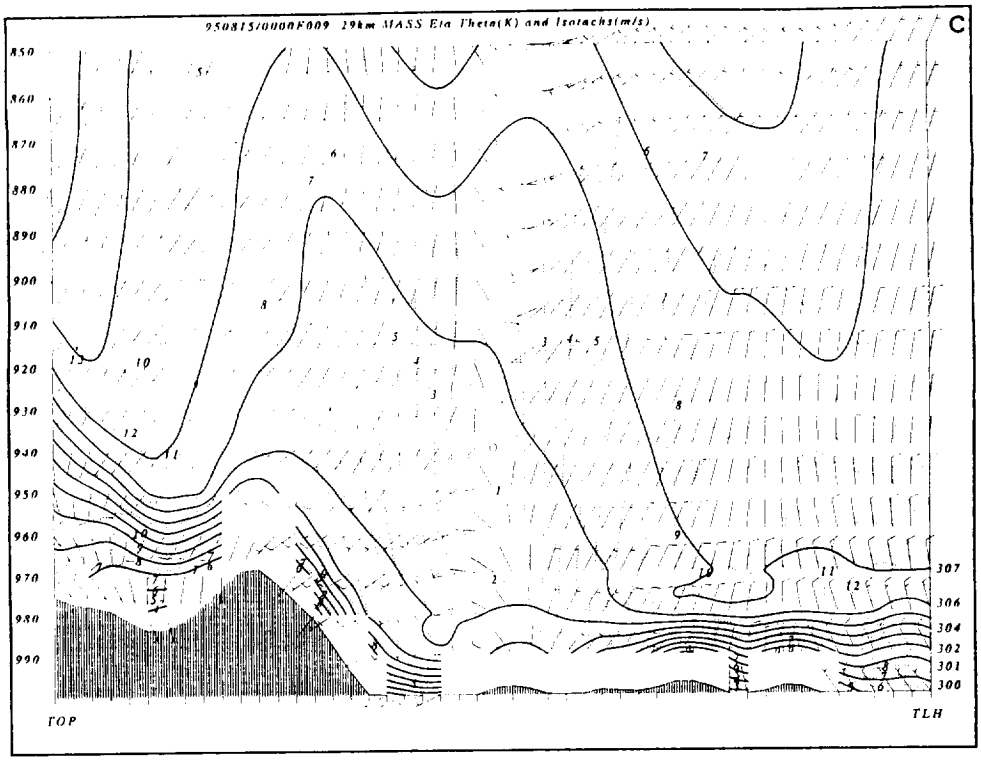
950815/0000F009 29km MASS Eta Theta(K) and Isotachs(m/s)
C
850
860
870
880
890
900
910
920
930
940
950
960
970
980
990
307
306
304
302
301
300
TOP
TLH

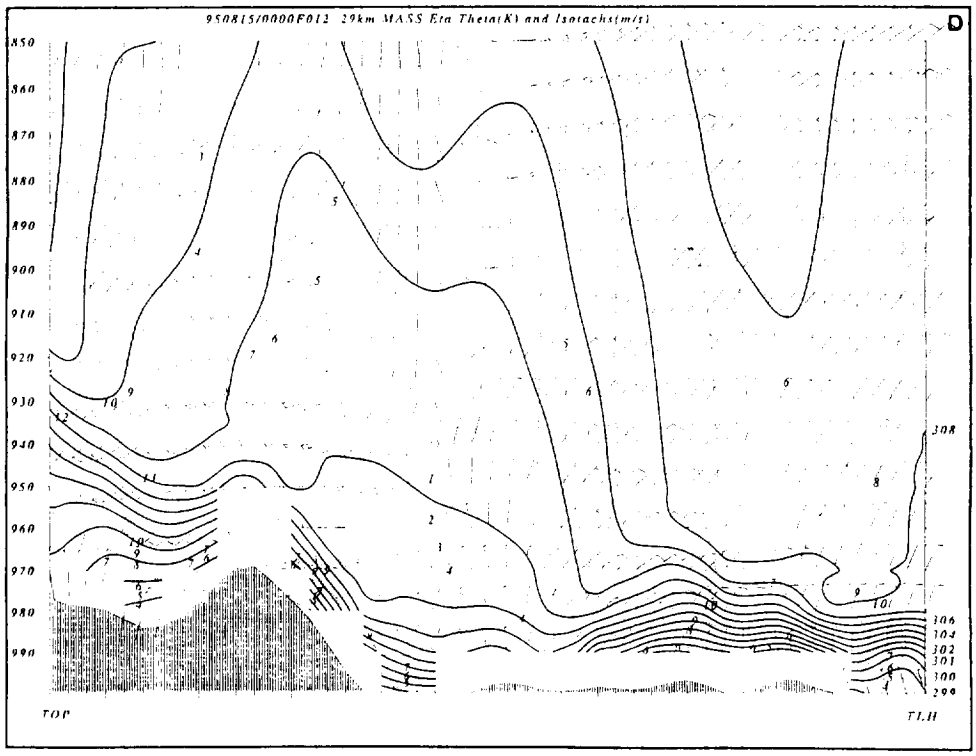
950815/0000F012 29km MASS Eta Theta(K) and Isotachs(m/s)
D
850
860
870
880
890
900
910
920
930
940
950
960
970
980
990
308
306
304
302
301
300
298
TOP
TLH